Optical role of diatom shell

2022-11-22

Authors describe the optical function of diatom shells: improve light distribution and availability inside the shell, and increase photosynthesis by up to 10%.

This file contains …

1. Science daily summary

2. Original article

3. Supplementary material

ScienceDaily®
Your source for the latest research news

Glass-like shells of diatoms help turn light into energy in dim conditions

Date: November 22, 2022

Source: Optica

Summary: A new study has revealed how the glass-like shells of diatoms help these microscopic organisms perform photosynthesis in dim conditions. A better understanding of how these phytoplankton harvest and interact with light could lead to improved solar cells, sensing devices and optical components.

FULL STORY

A new study has revealed how the glass-like shells of diatoms help these microscopic organisms perform photosynthesis in dim conditions. A better understanding of how these phytoplankton harvest and interact with light could lead to improved solar cells, sensing devices and optical components.

"The computational model and toolkit we developed could pave the way toward mass-manufacturable, sustainable optical devices and more efficient light harvesting tools that are based on diatom shells," said research team member Santiago Bernal from McGill University in Canada. "This could be used for biomimetic devices for sensing, new telecommunications technologies or affordable ways to make clean energy."

Diatoms are single-celled organisms found in most bodies of water. Their shells are covered in holes that respond to light differently depending on their size, spacing and configuration. In the journal *Optical Materials Express*, the researchers, led by McGill University's David V. Plant and Mark Andrews, report the first optical study of an entire diatom shell. They analyzed how different sections of the shell, or frustule, respond to sunlight and how this response is connected to photosynthesis.

"Based on our findings, we estimate that the frustule can contribute a 9.83 percent boost to photosynthesis, especially during transitions from high to low sunlight," said Yannick D'Mello, first author of the paper. "Our model is the first to explain the optical behavior of the entire frustule. So, it contributes to the hypothesis that the frustule enhances photosynthesis in diatoms."

Combining microscopy and simulation

Diatoms have evolved for millions of years to survive in any aquatic environment. This includes their shell, which is composed of many regions that work together to harvest sunlight. To study the optical response of diatom frustules, the researchers combined computer optical simulations with several microscopy techniques.

The researchers began by imaging the architecture of the frustule using four high-resolution microscopy techniques: scanning near-field optical microscopy, atomic force microscopy, scanning electron microscopy and dark field microscopy. They then used these images to inform a series of models that the researchers built to analyze each part of the frustule via 3D simulations.

Using these simulations, the researchers examined how different colors of sunlight interacted with the structures and identified three primary solar harvesting mechanisms: capture, redistribution and retention. This approach allowed them to combine the different optical aspects of the frustule and show how they work together to aid photosynthesis.

"We used different simulations and microscopy techniques to examine each component separately," said D'Mello. "We then used that data to build a study of how light interacts with the structure, from the moment it gets captured, to where it gets distributed after that, how long it is retained, and until the moment it likely gets absorbed by the cell."

Boosting photosynthesis

The study revealed that the wavelengths with which the shell interacted coincided with those absorbed during photosynthesis, suggesting it could have evolved to help capture sunlight. The researchers also found that different regions of the frustule could redistribute light to be absorbed across the cell. This suggests that the shell evolved to maximize the exposure of the cell to ambient light. Their findings also indicated that the light circulates inside the frustule long enough to aid photosynthesis during periods of transition from high to low illumination.

The new frustule model could make it possible to cultivate diatom species that harvest light at different wavelengths, allowing them to be customized for specific applications. "These light harvesting mechanisms of diatoms could be used to improve the absorption of solar panels by allowing sunlight to be collected at more angles, therefore partially removing the dependency of the panel to directly face the sun," said Bernal.

The researchers are now working to refine their model and plan to apply their new toolkit to study other species of diatoms. After that, they plan to extend the model beyond the light interactions within a single frustule to examine behaviors between multiple frustules.

This work commemorates Dan Petrescu, who passed away last year. The research would not have been possible without his insights, assistance and dedication.

Story Source:

Materials provided by **Optica**. *Note: Content may be edited for style and length.*

Journal Reference:

1. Yannick D’Mello, Santiago Bernal, Dan Petrescu, James Skoric, Mark Andrews, David V. Plant. **Solar energy harvesting mechanisms of the frustules of Nitzschia filiformis diatoms**. *Optical Materials Express*, 2022; 12 (12): 4665 DOI: 10.1364/OME.473109

Research Article | Vol. 12, No. 12 / 1 Dec 2022 / Optical Materials Express 4665
Optical Materials EXPRESS

Solar energy harvesting mechanisms of the frustules of *Nitzschia filiformis* diatoms

YANNICK D'MELLO,[1,*] SANTIAGO BERNAL,[1] DAN PETRESCU,[2] JAMES SKORIC,[1] MARK ANDREWS,[2] AND DAVID V. PLANT[1]

[1]*Department of Electrical and Computer Engineering, McGill University, Montreal, Quebec, Canada*
[2]*Department of Chemistry, McGill University, 845 Sherbrooke St W, Montreal QC H3A 0G4, Canada*
[*]*Yannick.DMello@mail.McGill.ca*

Abstract: Diatoms are major contributors to the global oxygen and carbon cycles. Their ability to thrive on photosynthesis, even in low and intermittent lighting conditions, is attributed to the optical response of the frustule, among other factors. However, how the frustule functions as a biophotonic feature is unknown. Using a toolkit consisting of numerical models and four microscopy techniques, we evaluated the optical response of frustules belonging to the species *Nitzschia filiformis*. Localized regions of the frustule exhibited functionalities including diffraction, lensing, waveguiding, circulation, filtering, resonances, and dispersion control. We show that these functionalities are complementary to each other in contributing to the solar energy harvesting mechanisms of capture, redistribution, and retention. In this context, frustule performance is evidently enhanced by perturbations to its sub-wavelength structure. We therefore modeled the frustule as a photonic circuit from which we estimated a contribution of approximately 9.83% to photosynthetic activity. To our knowledge, this represents the first model of the entire frustule, including its inherent disorder and the complementary behavior of localized optical functionalities. This provides quantitative support to the hypothesis that the frustule enhances photosynthesis in the cell. It supports the case for cultivating diatoms as sustainably mass-manufacturable devices with applications in solar energy, carbon sequestration, sensing, medicine, and metamaterials.

1. Introduction

It has been argued that in the next decade, natural systems alone could mitigate some 37% of the green house gas emissions necessary to limit global warming to 2°C [1]. Photosynthesis is the dominant natural process used to sequester organic and inorganic carbon from CO_2, thereby releasing oxygen that sustains life forms. In accomplishing this, photosynthesis utilizes 8 times as much solar energy as the current overall energy consumption by human society [2]. Studies on primary productivity estimate that almost half of all photosynthetic activity can be attributed to phytoplankton [3], of which the most common types are unicellular micro-organisms known as diatoms [4]. Diatom photosynthesis yields around 25% of atmospheric oxygen [5] and 40% of oceanic carbon fixation [6]. In this context, understanding how diatoms couple photons to drive photosynthetic processes, would directly inform and enhance technological developments in both solar energy harvesting [7] and carbon sequestration [8].

The proliferation of diatoms is partly due to their capacity for exponential growth, which indicates their potential to produce reproducible, tailored optical device constructs with yields far beyond current manufacturing technologies [9,10]. Combined with an ability for niche differentiation, diatoms have spawned more than 100,000 species that are distributed across almost every type of aquatic habitat [4]. The modern diatom is a result of 150 million years of evolution [11] with cell division occurring daily under favorable conditions [4]. Yet despite such a large genetic diversity, diatoms have similar characteristics. These similarities indicate a convergence of the corresponding evolutionary processes. For example, every species assimilates

#473109 https://doi.org/10.1364/OME.473109
Journal © 2022 Received 16 Aug 2022; revised 13 Oct 2022; accepted 29 Oct 2022; published 22 Nov 2022

Optical Materials EXPRESS

silicic acid monomers [12] into a hydrated, biosilica cell wall known as a frustule [13], which contains the protoplasm. Commonly, identification of the radial or bilateral symmetries of the frustule leads to non-phylogenetic classifications of diatoms into centric or pennate types, respectively [4]. In certain species of diatoms, the outer cell wall, or frustule, appears to offer mechanical protection [14], chemical buffering [15,16], and optical manipulation [7].

Diatoms are found in the euphotic zone, that is, the upper layers of water which are shallow enough to allow the penetration of sunlight, but turbulent enough to continually disturb the orientation of suspended diatoms. In such circumstances, the cell cannot easily maintain maximal exposure to incident sunlight as compared to terrestrial plants. The resulting low and intermittent illumination imposes a strong requirement on the cell to harvest sunlight efficiently. Although diatom pigments, antenna complexes, and photosystems have been found to assist photosynthesis [17,18], their collective contribution still does not explain the photosynthetic conversion efficiency of diatoms [7]. This suggests the presence of light harvesting mechanisms that mediate interactions at the interface between the chloroplasts and the optical field. These mechanisms are embedded in the optical properties of the frustule, which has been shown to facilitate the capture and redistribution of photosynthetic active radiation (PAR) [19–22]. In some pennate and centric diatoms this capability has been attributed to photonic crystal (PhC) [10,23–29] and lens [21,30–34] behavior that appears to be determined by the sub-wavelength architecture of the frustule. However, analysis of the individual optical components does not explain how they are recruited by the frustule as a whole, i.e., at a systems level, to enhance photosynthesis. Therefore, there is a need to identify and analyze the different optical mechanisms at play in the frustule which collectively govern its overall optical response [7,22]. We therefore seek to understand how the optical functionalities of the diatom frustule conjoin to harvest PAR for the chloroplasts in the cell.

The frustule is a micron-scale silica structure that is formed by active transport of monosilicic acid into a silica deposition vesicle from which it is eventually extruded. The frustule resembles a decorative pillbox, comprising a top and bottom valve united by one or more girdle bands. The silica is perforated with lattices of nanoscale holes (or areolae) causing a somewhat periodic modulation of the refractive index that results in a PhC response [27] to PAR [28]. PhCs have been widely designed and fabricated as optical device constructs for on-chip optical manipulation because they provide functional attributes like waveguiding [35], diffractive coupling [36], dispersion engineering [37], lensing [38], and spectral filtering [39,40]. Unsurprisingly, it has been speculated that the PhC features of diatom frustules might have evolved for cellular PAR manipulation [27,41]. Interpreting the frustule PhC architecture in a simplified model of square or hexagonal lattices, the patterned shell has been shown to host guided modes [27,28], resonant bands [25], pseudo-gaps [10], and radiation modes [27]. Valuable as these simplified models are, frustules exhibit nonuniformities in lattice pore size and distribution, and in other morphological features like silica valve thickening and tapering [25,42–44]. These nonuniformities have been associated with shifts in transmission wavelengths [25] and the presence of quasi-stop bands for blue light absorption [44]. Although nonuniformities and disorder are characteristic of the PhC-like properties of diatom frustules, their effect on the optical response has not been investigated even though there is good reason to probe the effect of disorder on PhC properties. For example, when fabricated as optical devices, disordered PhCs (DPhCs) exhibit diffused illumination and enhanced absorption [45,46], phenomena that might find correspondence with the observed redistribution of light in frustules [19]. In photonic technologies, spatial variations in PhC lattices have been used to guide propogating modes [47] and DPhCs have been intentionally introduced in devices to customize performance, broaden resonance bandwidth, or improve tolerance [48]. These properties increasingly resemble those of the naturally occurring DPhCs observed in some diatom frustules [37]. Recent advances in metalens design might also explain the wavelength-selective [26,49,50] and wide-angle [31] focusing [30,31,34,51] of DPhCs in the

Optical Materials EXPRESS

valve. The potential benefits of these DPhCs to the micro-organism are not known because the optical response of the frustule itself has not been extensively evaluated. For example, the valves of some centric diatoms have been shown to focus light entering the cell and to back-scatter light escaping the cell [19,31]. This type of asymmetric optical response suggests that the valves might facilitate transmission to the cell and retention inside it. In the whole frustule, the combination of upper and lower valves might be viewed as a Fabry-Perot cavity [52] whose purpose is to retain light. This view aligns with observations of enhanced absorption of 420 nm light in the region of the quasi-stop band of the frustule of *Melosira varians* [44]. Similarly, the frustule asymmetry in the centric diatom *Coscinodiscus granii* was proposed to not only enhance absorption, but that structures internal to the cell wall behave as diffraction gratings to redistribute incident light more evenly to the organism, particularly the chloroplasts and auxiliary pigments [19]. Despite the increasing sophistication of optical experiments on diatoms, our understanding of the relationship between the complex optical and biological functionalities of the frustule is still evolving [7]. For example, the way that the valves and girdle bands interact in the transport and scattering of light [53] has not yet been explored in much detail to determine how they collaborate as part of the sunlight harvesting mechanism. Moreover, little attention has been paid to the role of disorder in the frustule silica framework and how DPhC features might assist in the coupling and redistribution of light.

In the present work, we combine experimental measurements of an entire frustule construct with numerical simulations of its individual optical functionalities to provide a level of integration between frustule form and optical function. Our study focuses on the pennate, biraphid diatom species *Nitzschia filiformis*. This benthic species inhabits sediments in lake beds where its motility enables it to position itself at the most beneficial light penetration depth to optimize light exposure [54]. The frustules were studied using our previously developed toolkit comprising 4 microscopy techniques with complementary simulations [55] combined with our process for connecting photonic band diagrams to sub-wavelength features [56]. Our preliminary investigations of *N. filiformis* frustules revealed various PhC lattice configurations across the valve [28]. Here, we use this toolkit to identify and analyze a number of localized optical functionalities across the frustule and map them to the overall optical response. To determine the combined effect of the different optical processes at work, we model the frustule as an optical circuit, treating it as an ellipsoidal optical cavity embedded with these functionalities. Our model establishes how the individual optical functionalities might combine to yield three solar energy harvesting mechanisms of capture, redistribution, and retention, which enhance photosynthesis in the cell.

2. Methods

Diatom cells of the species *N. filiformis* were obtained from the Culture Collection of Algae at the University of Texas at Austin (UTEX). The exenic samples were cultivated in a modified growth medium under illumination by a diurnal light/dark cycle. The light sources were a 1:1 mix of cool and warm fluorescent lamps which were placed above the samples. Air exchange was achieved by passive diffusion into Erlenmeyer flasks with minimal agitation to prevent breaking the frustules. This arrangement simulates a benthic environment that is characteristically absent of strong currents. Bacterial accumulation was minimized by occasional aseptic transfers once a threshold cell count and average frustule size were obtained. The threshold cell concentration ensured that a sufficient population was available for imaging. Samples of frustules were cleaned and imaged based on previously established protocols [55]. A mixture of oxidizer consisting of 3 parts concentrated sulphuric acid and 1 part 30% hydrogen peroxide (piranha) was used to clean the silica frustules of cellular organic material. The valves and girdle were typically detached by the oxidizing agent.

An FEI Quanta 450 FE-ESEM scanning electron microscope (SEM) located at the Facility for Electron Microscopy Research at McGill University was used to obtain 126 images from 3

Optical Materials EXPRESS

different cell cultures over a period of 2 years. One of these cultures was grown in-house using the previously described protocols. For imaging, the frustules were drop-casted onto a coverslip and coated with a 5-10 nm layer of Pt. Frustule dimensions were measured from 43 SEM images which detailed 22 valves and 25 girdles. The dimensions and topography of the cleaned frustules were cross-verified with whole diatoms to ensure that the separated frustule components were not damaged by the cleaning process. From the SEM images, the 3D frustule architecture was reconstructed with a computer aided design (CAD) model using Autodesk Inventor, which was used for visualization purposes. Since the occurrence of multiple girdles was indicative of a diatom undergoing cell division, the model comprised of only a single girdle. The surface areas of the valves and girdles were estimated by using rectangular prisms with only 5 and 4 faces, respectively. The elemental composition of the frustule was determined by energy dispersive X-ray analysis (EDX) in the SEM.

The optical response of different regions of the frustule was simulated using the 3D finite difference time domain (FDTD) method in Ansys Lumerical FDTD. The bandwidth of the optical source was matched to the solar spectrum at sea level. The structure was excited by light sources including plane waves and optical dipoles inside the biosilica. The core material was set as silica with a refractive index of 1.45 [57] to represent the hydrated biosilica material of the frustule. The cladding was set as water at 20°C with a refractive index of 1.33 [57] corresponding to the inner cytoplasm and outer benthic environment of *N. filiformis* [54]. To simulate the response of the girdle, the central region of the frustule was flattened into a planar slab. The in-plane regions of the frustule were emulated using periodic boundary conditions. The external environment was represented by perfectly matched layers at the top and bottom boundaries. For simulations of the entire frustule, the DPhCs and arrays of holes were substituted by birefringent materials using effective medium theory [10,58,59] in order to lower the mesh resolution and therefore reduce the computation time.

The positions and diameters of the holes in the central lattice were mapped from the contrast of the SEM images [42]. Their corresponding point pattern was reconstructed as a lattice. The three main lattice parameters were measured by Delaunay triangulation. The distance between each pair of holes was measured as the localized pitch and cut-off at 450 nm to remove extended connections at the edges. The longitudinal pitch was measured along the length of the frustule and the lateral pitch was measured along its width. Their distributions revealed the extent of anisotropy in the lattice. The position of each hole was used to measure the angles between triplets of neighboring holes. To analyze the effect of variations in the lattice, each triad of holes was evaluated as an extended PhC using the supercell approximation [60], which produced one corresponding photonic band structure. Using a similar approach as that previously used to analyze quasi-periodic vibrational signals [61], these photonic band diagrams were then combined into an ensembled average, which revealed the effective photonic band structure of the DPhC.

Scanning, near-field optical microscopy (SNOM) and concurrent atomic force microscopy (AFM) measurements were performed using a WITec Alpha 300S microscope. The SNOM was operated in transmission mode [62], that is, with light coupled to the sample by the aperture in the near-field and collected by the bottom lens in the far-field. In this configuration, light passed from the upper objective through the aperture to the sample and was collected by the lower objective lens. Light was transmitted through an objective lens with NA 0.4 and strength 20x onto an apertured SNOM probe tip. The tip was magnetically attached to a cantilever below the lens and kept at a fixed angle. The inner diameter of the aperture was either 90 nm or 150 nm and its Al walls were 100 nm thick. This size was large enough to facilitate evanescent coupling into the sample yet small enough to resolve the individual holes of the PhC. At the aperture, an evanescent field interacted with the fine structure of the sample to convert it to a propagating wave [63,64]. These propagating waves were collected in the far field by a 60x, 0.8 NA lens

Optical Materials EXPRESS

below the sample and detected by a photomultiplier tube connected to an oscilloscope. Pixels in the image were collected 35 nm apart over a duration of 0.5 s per datapoint. The setpoint, power gain, and current gain for the AFM feedback were set at 2 V, 4%, and 4% respectively. The near-field response was further correlated with the topography of the sample using AFM. The SNOM was operated at two wavelengths – red at 660 nm (or 454 THz) and green at 518.9 nm (or 577 THz) using laser diodes LP660-SF60 and LP520-SF15, respectively, from Thorlabs. Blue wavelengths were not accommodated by the lensing system as explained in Supplement 1. Both diodes were operated by a laser mount LDM9LP connected to a controller LDC ITC 4001. There was no analyzer placed before the detector to separate polarizations [62].

Dark field microscopy (DFM) measurements were conducted using a Cytoviva Hyperspectral Imaging system. This configuration used a beam of normal incidence. A Tungsten source illuminated the valve with a white light spectrum within the wavelength range of 400-1000 nm (or 299-749 THz).

The microscopy images represented the highest resolution obtainable with the given instrumentation.

3. Results

3.1. Architecture

The biosilica frustule consisted of two bilaterally symmetric valves which were separated by one or more girdle bands [4]. It was reconstructed from SEM images as depicted in Fig. 1. The reconstructed model was verified by images of uncleaned samples and observations of live cultures under an optical microscope. The following reported dimensions refer to the average values of each measurement. Both valves and girdle exhibited a relatively uniform thickness of 400 nm. Only the region around the raphe was thicker than the rest of the frustule. The average height of the valve and girdle were 1.6 µm and 1 µm respectively. The overall height of the frustule depended on the number of girdle bands between the valves. Its length and width were determined by the girdle, which was 110 ± 10 µm and 4 ± 1 µm, respectively.

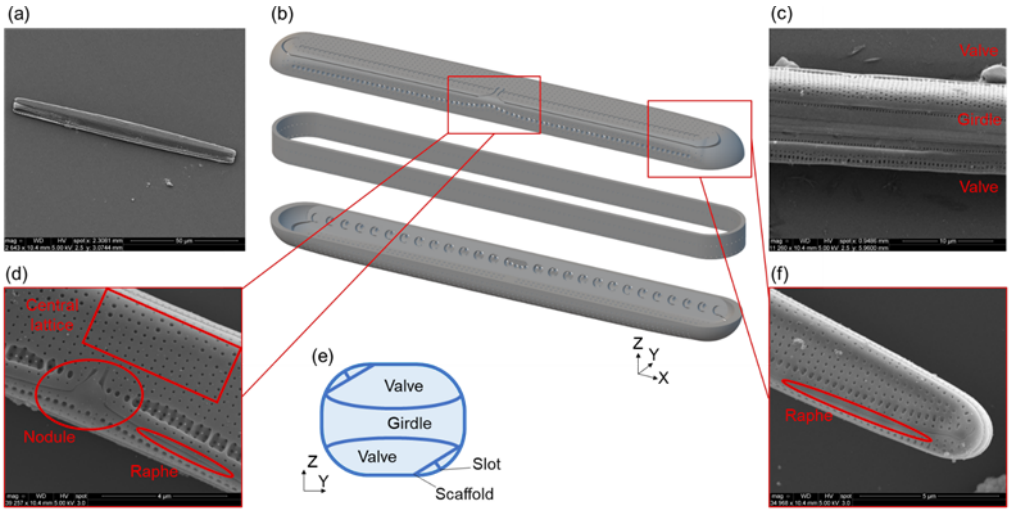

Fig. 1. Architecture of the frustule. (a) SEM of a frustule. (b) Exploded 3D CAD model of the frustule. (c) SEM of a side. (d) Central region of the valve. (e) Schematic of the cross-section. (f) Tail.

The valves occupied approximately 78% of the exposed surface area of the frustule. They were flat with curved sides and tapered at the ends to connect to the girdle. Each valve hosted a raphe

Optical Materials EXPRESS

on one side such that the raphes were diagonally opposite to each other as shown in Fig. 1(e). The raphe consisted of two, 25-nm-wide slits which spanned almost half the length of the valve from the central nodule to the tail as shown in Fig. 1(d). Although the slits could compromise the structural integrity of the valve, they appeared to be scaffolded by a series of inner protrusions underneath it. The flat region was perforated by a central lattice of holes, which terminated at the raphe and edges. Similarly spaced holes were present alongside the raphe albeit with larger diameters. The girdle also exhibited rows of holes with the same diameter and spacing as the central lattice.

By EDX, the elemental composition of the frustule yielded 39% Si, 52% O, and 9% C, along with traces of Cu and Fe. The dominant phase is silica, while the presence of C can be attributed to organic species incorporated in the porous silica matrix during the frustule production [65]. We approximated the refractive index, n, as that of bulk silica [10] (this is validated in Supplement 1). Its absorption was assumed to be low enough to incur negligible loss over the duration of the transient optical response. Due to the low refractive index contrast with the surrounding water and inner cytoplasm, as well as the thinness of the frustule, optical confinement was weak. This condition improved coupling to the cell [19,24] (see Supplement 1 for details).

3.2. Central lattice

The central lattice, shown in Fig. 2(a), spanned most of the surface area of the valve. Its localized parameters were mapped in Fig. 2(b) to reveal a DPhC with longitudinal periodicity and randomized perturbations. The measurements in Fig. 2(c,d) confirmed that the diameter and spacing of the holes were distributed about a mean value. Hole diameters were 80 ± 10 nm with a spacing of 300 ± 30 nm corresponding to the width of the striae, that is, the lateral columns of pores of along the valve. Each triad of neighboring holes subtended a slightly different angle as seen in Fig. 2(e). This gave rise to interspersed square and triangular lattice symmetries resulting in a generally hybrid, 'oblique' configuration. Any variations in the PhC proportionally altered its photonic band structure [25], as shown in Supplemental Fig. S2. The underlying photonic band structure of the DPhC is shown in Fig. 2(f) as an ensemble average of the photonic band structures obtained from each triad of holes [42] (see Methods). Its corresponding photonic density of states (DOS) is shown in Fig. 2(g).

In this ensemble average, multiple bands are present in the PAR wavelength range of 400-800 nm (or 375-749 THz) [19,22]. Two guided modes are represented by the adjacent, parallel bands in the light cone between the X-M symmetries and wavelengths of 650-800 nm (or 375-461 THz). The gap between these bands is negligible due to the small hole diameters and low index contrast of the DPhC. This enables evanescent coupling between them, which effectively combines their field distributions and DOS. The physical significance of a combined mode field distribution is a higher probability of overlap with incident light and therefore higher coupling to the structure, which was supported by longer photon lifetimes due to the combined DOS [27] (see Supplement 1). The effect is even more prominent in the quadruple degeneracy at the Γ point (k=0) around 440 nm (or 681 THz), which results in a heavily smoothed mode field distribution and high DOS. The reduced slopes of the bands at the pseudogap [10] also indicate a lower group velocity and therefore stronger light-matter interaction. Since these bands above the light cone represent radiation modes, their large number indicates that a variety of wavevectors are available for coupling [27].

The consequence of perturbations in the lattice is an effective 'smearing' of its corresponding photonic band structure as shown in Fig. 2(f). As a result, a larger range of wavelengths and wavevectors is accommodated by each band, and the DOS is spread out, especially at the peaks. This broadens the bandwidth and widens the acceptance angles of the modes and resonances in the DPhC. The improvement in its response is also evident from the DOS shown in Fig. 2(g), which correlates with the absorption spectrum of the chloroplasts [19,44,66] better than for the

Optical Materials EXPRESS

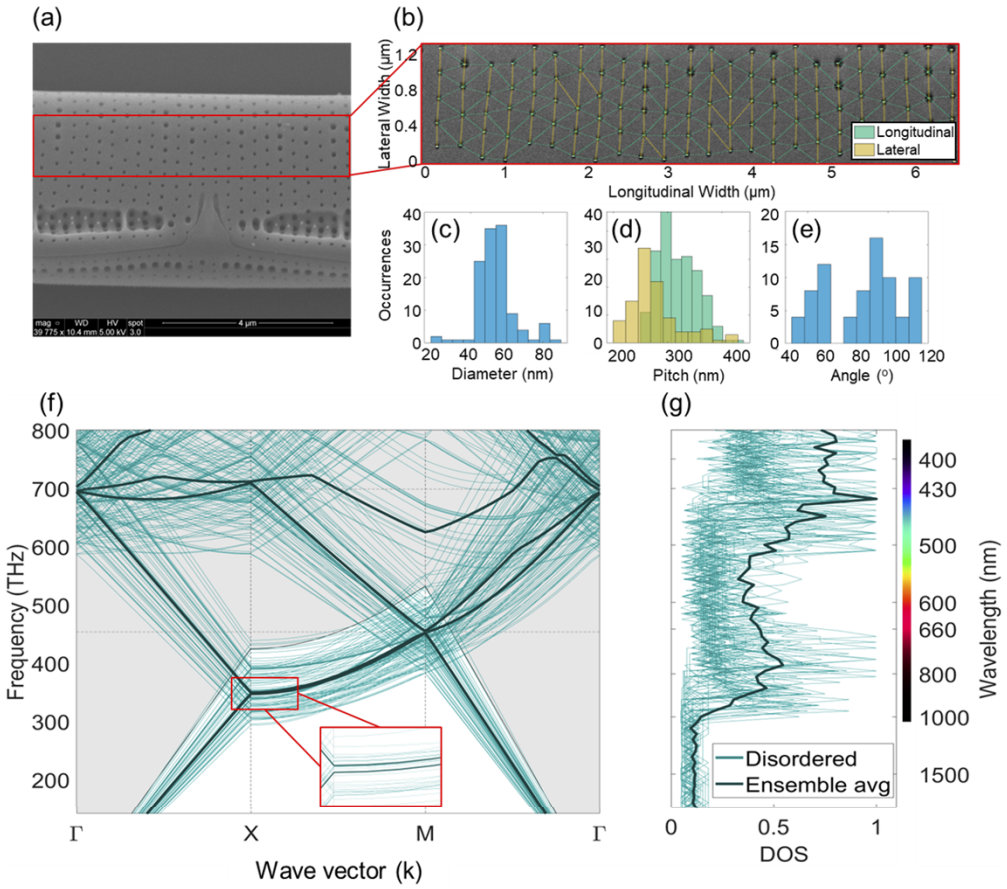

Fig. 2. Ensemble averaged photonic band structure of the central lattice. (a) Central region of the valve with a (b) zoom-in of the lattice showing (green) longitudinal and (yellow) lateral spacing. (c) Measured hole diameters, (d) longitudinal and lateral spacing, and (e) angles between holes. (f) Photonic band diagrams and (g) corresponding DOS of each triad of holes with an ensemble average showing the effective optical response. In (f), the shaded gray area indicates the light cone and inset shows the adjacent guided modes.

Optical Materials EXPRESS

case of a regular PhC [28]. This shows how disorder in the central lattice contributes to the PAR capture mechanism of the frustule, which could enhance photosynthetic conversion in the chloroplasts (this subject is elaborated in Supplement 1). Such a response might also provide photoprotection during periods of high illumination by restricting light at the frustule [26,67–69] so that it does not damage the chloroplasts.

Figure 3 shows the concave interior of the valve. The uniform background is due to the cover slip on which it the valve was placed. The localized optical response of the central lattice was examined by SNOM and concurrent AFM as shown in Fig. 3(b,c) and Fig. 3(e,f), respectively. At each position, the contact between the probe tip and the sample was verified by the AFM image and referenced with the topography observed in SEM images. In this way, the AFM and SEM images complemented each other. The blurred regions at the edges of the valve were caused by the limitation of the probe tip in accessing regions of high curvature. The edge of the valve was found to be 1.2 µm higher than at the center. Our analysis and interpretation of the SNOM data are explained in Supplement 1. The parallel, bright lines in the central lattice are spaced 300 nm apart as shown in Fig. 3(f). These correlate with the guided modes in the band diagram at 660 nm (or 454 THz). Their lateral orientation confirms that light was diffracted into lateral circulation by the longitudinal periodicity of the lattice. This also explains the brightness at the edges of the valves in the SNOM image in Fig. 3(f) and the dark field microscopy (DFM) image in Fig. 3(d).

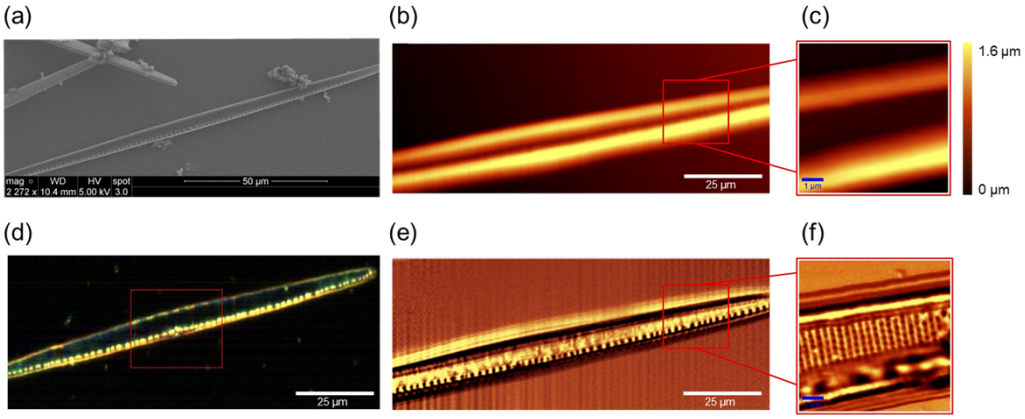

Fig. 3. Microscope images of the interior of a valve. (a) SEM, (b) AFM with (c) a zoomed-in region, (d) DFM, (e) SNOM at a wavelength of 660 nm with (f) a zoomed-in region. The SNOM and AFM images were obtained concurrently for (b) and (e) as well as (c) and (f).

In DFM, the light source was blocked so that only scattered light reached the detector. This contrasts with SNOM which only detects transmitted light. DFM therefore imaged the far-field response of the DPhC, whereas SNOM imaged the near-field response. In this sense, the images produced by DFM and SNOM are complementary to each other. The scattered light in the DFM image reveals the wavelength-dependent spatial distribution of the optical response, that is, it shows which wavelengths had interacted with the valve at a given location. As seen in Fig. 3(d), the central lattice exhibits a green hue, and the valve edges are yellow with traces of red. The green hue indicates that the 400-600 nm wavelength range (or 500-749 THz) from blue to yellow had coupled to radiation modes of the central lattice, which correlates with the band diagrams in Fig. 2(f). Note that coupling between the radiation modes and free space was bidirectional due to the optical reciprocity of biosilica. So, light that had coupled with the valve was subsequently radiated after a certain propagation length. This highlights the significance of the valve width, which was sufficiently narrow for laterally propagating light to reach the edges before it could be radiated. This phenomenon therefore contributes to the solar energy

Optical Materials EXPRESS

harvesting mechanism of retention. In a whole frustule, this light would continue to propagate into an adjoining girdle rather than be scattered from the edge of an isolated valve as in the DFM image. The brownish-yellow color at the edges implies that wavelengths above 560 nm (or 535 THz) either couple into it from free-space or are guided into it from the central lattice. The latter case correlatesd with the sequence of parallel, bright lines observed in the SNOM images in Fig. 3. Both cases correlate with the resonance points and guided modes in the band diagrams of Fig. 2(f). The high intensity observed around the raphe merits a deeper investigation of its optical response.

3.3. Raphe

The raphe consists of two longitudinal slits surrounded by a row of holes on either side and scaffolded by protrusions underneath it. Although the spacing between holes is the same as that of the central lattice and girdle, their diameters are about twice as large at 160 ± 15 nm. Since the raphe is known to facilitate locomotion [70], the larger diameter of the holes can be assumed to accommodate the secretion of material for propulsion [4] while the hole periodicity maintains the optical response of the central lattice. The inner protrusions are also periodically spaced. This region exhibits a particularly intense accumulation of yellow light in both DFM and SNOM images, a feature that indicates a high localized DOS (LDOS) [71]. Its behavior can be evaluated using the 1D band diagram shown in Fig. 4(c), which reveals a resonance at the yellow-red wavelengths. The lack of holes at the nodule and raphe creates defects in the DPhC giving rise to localized states [71].

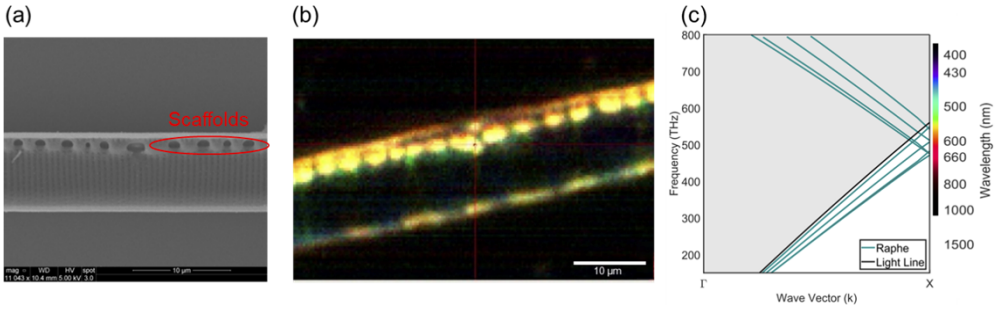

Fig. 4. Optical response of the region around the raphe. (a) The array of inner protrusions underneath the raphe. (b) Accumulation of yellow light at these protrusions (corresponding to the red box in Fig. 3(d)). (c) 1D photonic band diagram of this region.

At the raphe, yellow light accumulates at the protrusions along its length. This effect is attributed to the relative thickness of biosilica which increases the LDOS and enables the protrusions to act as temporary reservoirs of light. In this sense, the resonance of the rows of holes surrounding the raphe is supported by the retention of light in the protrusions underneath it. The accumulation of light in this region is therefore amplified by its high LDOS and low confinement, which contribute to retention of light in the frustule for the benefit of photosynthetic absorption in the cell.

3.4. Tail

The curvature of the tail resembled a tapered, lensed fiber. It was therefore assumed to enable butt-coupling between the frustule and free-space. Indeed, our simulations showed an insertion loss of 1.4 dB at 450 nm as shown in Fig. 5(c). The curvature exhibited in the tail region prevents the girdle from operating as a longitudinal racetrack resonator, as observed in some centric diatoms [19,29]. Once butt-coupled, the light propagates longitudinally, that is, along the length

Optical Materials EXPRESS

of the frustule. The pennate symmetry of the frustule implies that this light would be coupled out the opposite tail unless it was laterally redirected as it propagated. In fact, the light can be redirected by the longitudinal periodicity of the central lattice (described in section 3.2) and the rows of holes along the girdle (see section 3.5).

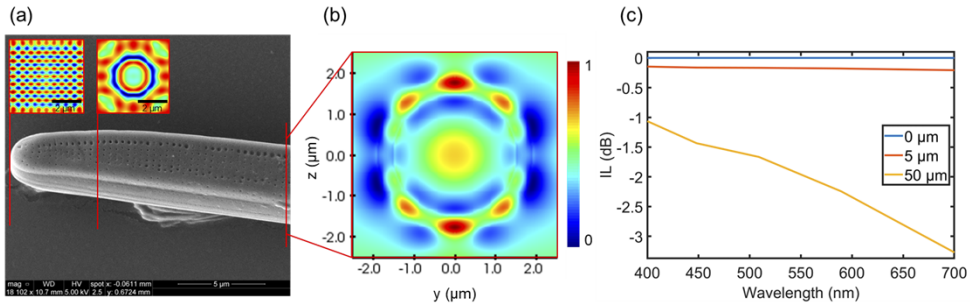

Fig. 5. Optical response of the tail. (a) The tapered, curvature of the tail with insets at the red slices showing the evolution of an incident plane wave as it butt-couples to the frustule. (b) Mode profile of the butt-coupled, confined light propagating longitudinally along the frustule. (c) Transmission spectrum at each of the red slices in (a).

3.5. Girdle

As shown in Fig. 6(a), the girdle band circumscribes and joins the top and bottom valves, and tapers towards the tails. We identified three ways in which light can enter the girdle: by coupling out-of-plane from either free space or the protoplasm, by butt-coupling longitudinally from the tails, or by being guided laterally from the valve edges. Out-of-plane coupling was assumed to be negligible because the girdle occupies only a fraction of the exposed surface area of the frustule.

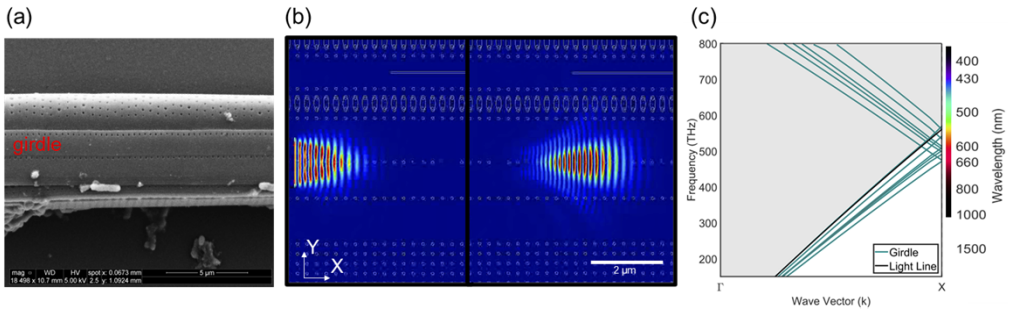

Fig. 6. Optical response of the girdle. (a) The array of holes along the girdle. (b) Diffraction of light by the holes during longitudinal propagation after (left) 27 fs and (right) 40 fs. (c) 1D photonic band diagram of the array of holes.

The holes in the girdle have a diameter of 78 ± 12 nm and are longitudinally spaced 213 ± 20 nm apart. This spacing matches the periodicity of the central lattice. The holes form a row in each girdle and are spaced approximately 820 nm, corresponding to adjacent girdles. This means that each row functions as an individual grating. Its length and periodicity impose a Bragg effect on longitudinally propagating light. We simulated this behavior as a 1D band diagram in Fig. 6(c), which reveals a collapsed bandgap within the wavelength range of 550-650 nm (or 461-545 THz). Perturbations in the rows of holes induced sufficient disorder to smear the 1D band diagram (as indicated by the multiple bands), thereby broadening its spectral and directional response

Optical Materials EXPRESS

[72]. The optical response is shown in Fig. 6(b) and relates to both remaining methods of light entry into the girdle, that is, longitudinally from the tail and laterally from the valves. Hence, as laterally circulating light reaches the girdle from the central lattice, the rows of holes restrict any longitudinal diffusion so that light is forced to traverse the girdle into the opposing valve. Additionally, as shown in Fig. 6(b), butt-coupled light from the tails is laterally diffracted by the row of holes. This reduces the amount of light that traverses the girdle longitudinally to the opposite tail. Since the light is incrementally redirected as it propagates down the longitudinal row of holes, this implies that the length of the row is an important factor in increasing the amount of light that is redirected. It is therefore assisted by the elongated, pennate shape of the frustule.

3.6. Frustule

The frustule comprises the central lattices, raphes, tails, and girdle. We studied their combined optical behavior to determine the overall response of the frustule. As a whole, the frustule behaves as an ellipsoidal silica shell in water [73] as shown in Fig. 7(b). It consists of a cylindrical racetrack (central lattices and girdle, Fig. 7(a)) which contains two diagonally opposite gratings (raphes) and is capped at both ends by tapered, hemispheric lenses (tails, Fig. 7(c)).

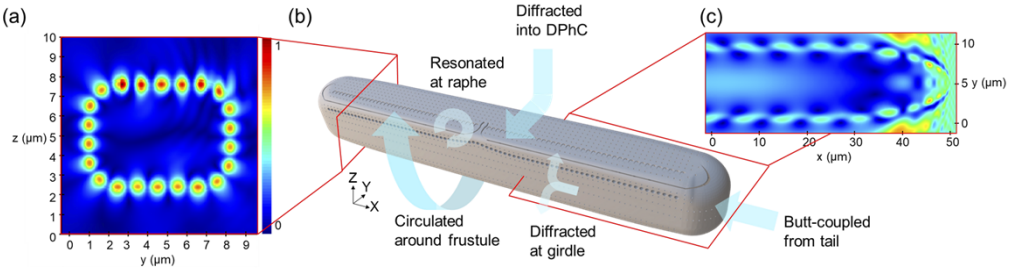

Fig. 7. Optical response of the frustule. (a) Racetrack hosting lateral circulation around the cross-section shown in Fig. 1(e). (b) Entire frustule with the blue arrows indicating the various directions of light propagation including lateral circulation, diffraction by the DPhC of the central lattice, diffraction by the row of holes in the girdle, resonance at the raphe, and butt-coupling into the tail. (c) Field distribution of butt-coupling at the tail of the frustule.

The frustule architecture hosts localized optical functionalities which contribute to the solar energy harvesting mechanisms of capture, redistribution, and retention. In our view, incident PAR can be captured by the radiation modes of the central lattice, butt-coupling from the tails as seen in Fig. 7(c), or at grazing incidence due to the relatively higher refractive index of biosilica. Light entering the frustule can be assumed to be immediately available for absorption by any chloroplast since even unabsorbed light was redistributed across the frustule to regions containing unsaturated chloroplasts. Light is laterally redirected by both the central lattice and rows of holes in the girdle. This light circulates laterally around the cylindrical cross-section of the frustule as seen in Fig. 7(a). The cross-section therefore can be interpreted as a lateral racetrack resonator with a Q factor of approximately 271 to 822 at wavelengths of 805 nm to 424.8 nm (or 372 THz to 706 THz), respectively. Within the racetrack, we identify additional methods to retain PAR. The DPhC hosts adjacent bands, band crossings, and pseudogaps, which increase the DOS and therefore photon lifetimes in the central lattice. Light from the central lattice is also accumulated by the rows of larger holes around the raphe, which appear to behave as a reservoir for photons. Our results suggest that the individual optical functionalities of the frustule complement each other to harvest PAR.

An analogous photonic circuit diagram of the frustule is shown in Supplemental Fig. S4 along with a derivation of the modelling approach. We considered the maximum absorption rate of the chloroplasts to be 3.98×10^{12} photons s^{-1} corresponding to an irradiance of 750 μmol

Optical Materials EXPRESS

photons m^{-2} s^{-1} [22]. When the irradiance exceeds this value, we assume that the excess photons would be retained in the frustule. However, when the irradiance is suddenly reduced to 550 µmol photons m^{-2} s^{-1}, then our calculations (as described in Supplement 1) indicate that the light retained in the frustule can contribute approximately 9.83% to absorption by the chloroplasts. This would enable photosynthetic activity to continue at reduced light levels. In this manner, our circuit model of the frustule depicts how its retention mechanism can supply photons to the cell during fluctuations in illumination and furthermore, how its harvesting mechanisms can improve the photosynthetic conversion efficiency of the cell during periods of low illumination.

4. Discussion

Diatoms exhibit unique light harvesting and energy dissipation mechanisms as compared to other phototrophs. Their proliferation even in harsh, low-light environments, has prompted numerous investigations to determine the solar energy harvesting mechanisms of the cell, including its photo-physiology and optical response. We evaluated the optical behaviour of frustules belonging to the species *N. filiformis*. The architecture exhibited localized optical functionalities including diffraction, resonances, spectral filtering and waveguiding, polarization independence, and wide-angle coupling. The frustule itself acts as an ellipsoidal optical cavity which amplifies these effects. The optical response was strongest within the wavelength range of PAR, which suggests that the frustule could promote absorption of light by the chloroplasts [19,44,66]. Biological functionality is co-resident with optical functionality. For example, the holes accommodate the exchange of nutrients with the marine environment [13]. Larger holes around the raphe are also believed to assist locomotion [70].

The thinness and low refractive index of the frustule evokes large mode field distributions with a polarization independent response. This facilitates coupling to the chloroplasts and might even aid fluorescent resonant energy transfer between constituent pigments. Additionally, since both raphes are diametrically opposite each other in the cross-section of the frustule, the space between them is maximized. This space could allow the chloroplasts to cluster around each raphe during periods of darkness, which is supported by in vivo observations of chloroplasts moving within the cell. Our analysis of the DPhC in the central lattice proves that perturbations in the lattice hole periodicity are not only tolerated but may be beneficial (Supplement 1). This suggests that disorder might have evolved to enhance the light harvesting efficiency of the frustule. This could likely happen during the growth process which could be interpreted as a Turing reaction diffusion mechanism during self-organization. However, the processes involved in the structuring and composition modification of the frustule in response to environmental stimuli are yet to be determined [13]. Hence, it remains unproven whether this disorder in the lattice geometry is encoded in the genetic information of the cell, is naturally caused by defects that arise during synthesis, or are an adaptive response to environmental pressures [74]. Additionally, although these perturbations enhance the optical response, such an inference should not be misconstrued. Note that the optical behavior of the sub-wavelength architecture was primarily due to its periodicity, and only enhanced by the perturbations. This is not equivalent to the distortions caused by contamination or metabolic insertion [19], which can be fatal to the cell. We therefore infer that as with most natural systems, diatoms flourish when left to their own (optical) devices and are unlikely to benefit from human interference.

Our results confirm that localized regions of the frustule host specific optical functionalities, which when combined, indicates complementary behavior related to the mechanisms for harvesting PAR. This leads to our hypothesis that the frustule aids photosynthesis in the live cell. It could be validated by in vivo measurements of the photosynthetic conversion efficiency of the cell, ideally isolating the response with and without a frustule as well as for each of the three solar energy harvesting mechanisms. To support our hypothesis, we modeled the frustule as a photonic circuit and derived its contribution to photosynthesis for the first time. However, the model faces

Optical Materials EXPRESS

certain limitations based on its assumptions, which particularly do not account for the spectrally dependent response of the frustule and chloroplasts, the molecular adaptation of photosynthesis under fluctuating illumination, and a characterization of the effect of perturbations to the lattice. These limitations could be addressed by further development of the model in a follow-up study. Such a model could be directly applied to the design process for optical interfaces [37] such as photodiodes, grating couplers, and photovoltaic panels. Additionally, our toolkit for analyzing the optical response of the frustule could be applied to other species of diatoms that exhibit a similar architecture and composition. A large-scale study across different species would refine the model and produce a variety of novel insights by leveraging the architectural diversity of different species. This would pave the way for frustules to be used as passive, biomimetic devices in sensing and communications technologies.

Since diatoms are often found in clusters, it is valuable to consider the implications of our findings in the context of multiple neighboring diatoms. Our simulations indicate that the tapered end of the frustule functions as a butt-coupler. This behavior is similar to lensed fibers, which can be measured by their end-to-end coupling efficiency [75]. Based on the reciprocity of light, we infer that since the tail is capable of coupling light into the frustule, it is equally capable of coupling light out to free space, which could then be coupled into the tail of another frustule. A similar hypothesis may be made for evanescent coupling between adjacent frustules. It suggests that light may be transferred from one frustule to another, which would enable light to be shared between cells in clusters via butt or directional coupling. In fact, the optical interactions between cells could be tested by placing the frustules in the same configuration as fiber-to-fiber coupling experiments. The process might also be assisted by the sticky, excreted biofilm that affixes multiple frustules in close proximity to each other [4]. Such coupling would facilitate the redistribution of excess light across a cluster from areas of high illumination to darker areas. These findings allude to a strong evolutionary advantage of the frustule in maintaining the health of the entire cluster, even when under shadows from cloud cover, vertical mixing, or wave focusing. In this context, diatom frustules could be responsible for an even larger enhancement of photosynthesis than indicated by our single-cell model. An analysis of multiple adjacent diatoms could demonstrate the optical behavior of clusters behaving as a superlattice of frustules [23]. Such results could inform new approaches to developing solar energy farms or decentralized telecommunication networks. For example, silica-based PhCs have already been investigated as low-cost coating films to provide dust protection and light harvesting for photovoltaics [31,76].

Over millions of years of evolution, successive generations of diatoms seem to have perfected the ability to grow the custom optical tools that are necessary for their survival. A better understanding of their photonic toolbox offers significant implications for biomimetic technological development. Their potential as species-specific devices is further supported by a high adaptability via selective breeding, genetic diversity offering a variety of nanophotonic design constructs, and the compatibility of the biosilica frustule with semiconductor chip fabrication processes allowing them to be directly used as passive optical devices. Since the frustule of each species exhibits a unique combination of optical functionalities, the existence of over 100,000 species has significant implications for new nanophotonic paradigms. For example, the mechanical, biochemical, and optical characteristics of the frustule already allow it to be used as a meta-surface for biosensing [77], carrier for drug delivery [78], and template for solar energy conversion [7,20,79]. Furthermore, their ability to reproduce in exponentially increasing numbers at negligible cost could be leveraged toward mass manufacturing [9]. In this context, diatom frustules could already provide the basis for a nanophotonic, biomimetic platform which combines diatom frustules and silicon photonic chips to realize novel optical functionalities. This could accelerate development in solar cells [79], nano-antennas [41], biofuels [80], and sensing [77]. Since diatoms are light-activated carbon sequestration systems, the cultivation of diatoms alone could support research in carbon sequestration, oceanic health monitoring, biotechnology [9,80,81],

Optical Materials EXPRESS

and solar energy harvesting [7,81,82]. Such progress is needed to reduce climate change and accelerate progress toward a sustainable society, which diatom frustules can facilitate at a very high benefit-cost ratio.

5. Conclusion

Using a combination of SEM, AFM, SNOM, DFM, CAD modelling, and numerical modelling, we analyzed the optical response of the frustule belonging to the species *Nitzschia filiformis*. Its response was enabled by a higher refractive index of biosilica compared to the surrounding water and cytoplasm. A determining factor was the architecture, which behaved as an ellipsoidal micro-shell with localized, sub-wavelength features including DPhCs, gratings, a racetrack, and lenses. Each feature evoked specific functionalities including coupling, waveguiding, scattering, diffraction, spectral filtering, resonance, and dispersion control. Our analysis of perturbations in these features showed that the frustule can not only tolerate defects but actually exploit them to improve its robustness, bandwidth, and acceptance angles. Together, these functionalities contributed to PAR harvesting mechanisms of capture, redistribution, and retention. Our findings therefore suggest that the frustule could assist the absorption rate of chloroplasts to improve the photosynthetic conversion efficiency of the cell. We developed this hypothesis by modeling the frustule as a photonic circuit. Using it, we estimate that the optical response contributed to 9.83% of photosynthesis in the cell during periods of low, intermittent illumination. Furthermore, these apparently complementary functionalities could justify an evolutionary purpose for the optical response of the frustule. Our analysis of light harvesting mechanisms in the frustule further motivates the cultivation of diatoms for solar energy harvesting, carbon sequestration, and other technological applications.

Funding. NSERC Silicon Electronic-Photonic Integrated Circuits (SiEPIC) program; The Centre for Systems, Technologies and Applications for Radiofrequency and Communication (STARaCom); Faculty of Engineering, McGill University; Centre québécois sur les matériaux fonctionnels; CMC Microsystems; Fonds de recherche du Québec – Nature et technologies.

Acknowledgments. Our work commemorates Dr. Dan Petrescu who was an insightful researcher, enthusiastic collaborator, and close friend. It is dedicated to Dan's family and friends who are facing their own emotional ordeals in wrapping up his legacy. Additionally, the authors would like to thank Melissa Campbell, Nathalie Tufenkji Amy Blum, and Etienne Low-Decarie for their support, resources, and insights. Y. D'Mello would also like to thank Orad Reshef, Shai Tsesses, and Kathleen McGarvey for their insight and guidance.

Disclosures. The authors declare no conflicts of interest.

Data availability. Data underlying the results presented in this paper are not publicly available at this time but may be obtained from the authors upon reasonable request.

Supplemental document. See Supplement 1 for supporting content.

References

1. B. W. Griscom, J. Adams, P. W. Ellis, R. A. Houghton, G. Lomax, D. A. Miteva, W. H. Schlesinger, D. Shoch, J. V. Siikamäki, P. Smith, P. Woodbury, C. Zganjar, A. Blackman, J. Campari, R. T. Conant, C. Delgado, P. Elias, T. Gopalakrishna, M. R. Hamsik, M. Herrero, J. Kiesecker, E. Landis, L. Laestadius, S. M. Leavitt, S. Minnemeyer, S. Polasky, P. Potapov, F. E. Putz, J. Sanderman, M. Silvius, E. Wollenberg, and J. Fargione, "Natural climate solutions," Proc. Natl. Acad. Sci. **16**(4), 634–644 (2016).
2. U. Steger, W. Achterberg, K. Blok, H. Bode, W. Frenz, C. Gather, G. Hanekamp, D. Imboden, M. Jahnke, and M. Kost, *Sustainable Development and Innovation in the Energy Sector* (Springer Science & Business Media, 1988).
3. C. B. Field, M. J. Behrenfeld, J. T. Randerson, and P. Falkowski, "Primary production of the biosphere: integrating terrestrial and oceanic components," Science **38**(7), 1347–1364 (1993).
4. F. E. Round, *The Diatoms : Biology & Morphology of the General* (Cambridge University Press, 1995).
5. C. S. Rousseaux and W. W. Gregg, "Interannual variation in phytoplankton primary production at a global scale," Remote Sens. **37**(2), 245–266 (1990).
6. P. Tréguer, C. Bowler, B. Moriceau, S. Dutkiewicz, M. Gehlen, O. Aumont, L. Bittner, R. Dugdale, Z. Finkel, D. Iudicone, O. Jahn, L. Guidi, M. Lasbleiz, K. Leblanc, M. Levy, and P. Pondaven, "Influence of diatom diversity on the ocean biological carbon pump," Nat. Geosci. **46**(2), 335–351 (1999).

Optical Materials EXPRESS

7. J. W. Goessling, S. Yanyan, M. Kühl, and M. Ellegaard, "Frustule photonics and light harvesting strategies in diatoms," in *Diatom Morphogenesis* (1863), pp. 317–343.
8. K. Leblanc, B. Quéguiner, F. Diaz, V. Cornet, M. Michel-Rodriguez, X. D. d. Madron, C. Bowler, S. Malviya, M. Thyssen, G. Grégori, M. Rembauville, O. Grosso, J. Poulain, C. de Vargas, M. Pujo-Pay, and P. Conan, "Nanoplanktonic diatoms are globally overlooked but play a role in spring blooms and carbon export," Nat. Commun. **9**(1), 953 (2018).
9. N. Sharma, D. P. Simon, A. M. Diaz-Garza, E. Fantino, A. Messaabi, F. Meddeb-Mouelhi, H. Germain, and I. Desgagné-Penix, "Diatoms biotechnology: various industrial applications for a greener tomorrow," PLoS One **11**(5), e0155977 (2016).
10. J. W. Goessling, W. P. Wardley, and M. Lopez-Garcia, "Highly reproducible, bio-based slab photonic crystals grown by diatoms," Adv. Sci. **6**(2), 218–229 (2022).
11. P. G. Falkowski, M. E. Katz, A. H. Knoll, A. Quigg, J. A. Raven, O. Schofield, and F. Taylor, "The evolution of modern eukaryotic phytoplankton," Science **100**(C7), 13255–360 (1995).
12. J. Livage and P. J. Lopez, "Biogenic silica glasses," in *Encyclopedia of Glass Science, Technology, History, and Culture* (1996), pp. 891–906.
13. E. De Tommasi, J. Gielis, and A. Rogato, "Diatom frustule morphogenesis and function: a multidisciplinary survey," Mar. Genomics **35**, 1–18 (2017).
14. C. E. Hamm, R. Merkel, O. Springer, P. Jurkojc, C. Maier, K. Prechtel, and V. Smetacek, "Architecture and material properties of diatom shells provide effective mechanical protection," Nature **47**(6), 1637–1647 (2002).
15. A. J. Milligan and F. M. M. Morel, "A proton buffering role for silica in diatoms," Science **112**(26), 8008–8012 (2015).
16. S. H. Michelle and G. M. James, "Functional morphology of diatom frustule microstructures: hydrodynamic control of Brownian particle diffusion and advection," Geophys. Res. Lett. **44**(8), 3752–3760 (2017).
17. P. Kuczynska, M. Jemiola-Rzeminska, and K. Strzalka, "Photosynthetic pigments in diatoms," Mar. Drugs **13**(9), 5847–5881 (2015).
18. W. Wang, L.-J. Yu, C. Xu, T. Tomizaki, S. Zhao, Y. Umena, X. Chen, X. Qin, Y. Xin, M. Suga, G. Han, T. Kuang, and J.-R. Shen, "Structural basis for blue-green light harvesting and energy dissipation in diatoms," Science **363**(6427), eaav0365 (2019).
19. J. W. Goessling, Y. Su, P. Cartaxana, C. Maibohm, L. F. Rickelt, E. C. L. Trampe, S. L. Walby, D. Wangpraseurt, X. Wu, M. Ellegaard, and M. Kühl, "Structure-based optics of centric diatom frustules: modulation of the in vivo light field for efficient diatom photosynthesis," New Phytol. **168**, 43–56 (2018).
20. X. Chen, C. Wang, E. Baker, and C. Sun, "Numerical and experimental investigation of light trapping effect of nanostructured diatom frustules," Sci. Rep. **51**(3), 617–649 (1993).
21. E. De Tommasi, I. Rea, M. A. Ferrara, L. De Stefano, M. De Stefano, A. Y. Al-Handal, M. Stamenković, and A. Wulff, "Underwater light manipulation by the benthic diatom Ctenophora pulchella: From PAR efficient collection to UVR screening," Nanomaterials **59**(22), 6702 (2020).
22. J. W. Goessling, S. Frankenbach, L. Ribeiro, J. Serôdio, and M. Kühl, "Modulation of the light field related to valve optical properties of raphid diatoms: implications for niche differentiation in the microphytobenthos," Limnol. Oceanogr. **45**(3), 569–579 (2000).
23. Y. Owari, F. Nakamura, Y. Oaki, H. Tsuda, S. Shimode, and H. Imai, "Ultrastructure of setae of a planktonic diatom, Chaetoceros coarctatus," Sci. Rep. **36**(18), 4214 (1997).
24. E. De Tommasi, "Light manipulation by single cells: the case of diatoms," Appl. Opt. **25**(12), 1930 (1986).
25. K. Kieu, C. Li, Y. Fang, G. Cohoon, O. D. Herrera, M. Hildebrand, K. H. Sandhage, and R. A. Norwood, "Structure-based optical filtering by the silica microshell of the centric marine diatom Coscinodiscus wailesii," Opt. Express **42**(3), 526–15999 (2003).
26. S. Yamanaka, R. Yano, H. Usami, N. Hayashida, M. Ohguchi, H. Takeda, and K. Yoshino, "Optical properties of diatom silica frustule with special reference to blue light," J. Appl. Phys. **57**(8), 1777 (2018).
27. T. Fuhrmann, S. Landwehr, M. El Rharbi-Kucki, and M. Sumper, "Diatoms as living photonic crystals," Appl. Phys. B **65**(1), 173–190 (2020).
28. Y. D'Mello, S. Bernal, J. Skoric, D. Petrescu, M. Andrews, and D. V. Plant, "Photonic Crystal Behavior of Nitzschia Filiformis Phytoplankton for Chlorophyll A Photosynthesis," in *Conference on Lasers and Electro-Optics, OSA Technical Digest* (Optical Society of America, 2018), 2676.
29. S. Bernal, Y. D. Mello, D. Petrescu, M. Andrews, and D. V. Plant, "Optical response of the centric valve in cyclotella quillensis diatoms," in *2020 Conference on Lasers and Electro-Optics (CLEO)*, (2020), 1–2.
30. L. D. Stefano, I. Rea, I. Rendina, M. D. Stefano, and L. Moretti, "Lensless light focusing with the centric marine diatom Coscinodiscus walesii," Opt. Express **15**(7), 737–759 (1993).
31. J. Romann, J.-C. Valmalette, M. S. Chauton, G. Tranell, M.-A. Einarsrud, and O. Vadstein, "Wavelength and orientation dependent capture of light by diatom frustule nanostructures," Sci. Rep. **43**(6), 1107–1118 (1998).
32. E. De Tommasi, A. C. De Luca, L. Lavanga, P. Dardano, M. De Stefano, L. De Stefano, C. Langella, I. Rendina, K. Dholakia, and M. Mazilu, "Biologically enabled sub-diffractive focusing," Opt. Express **25**(4), 571–27227 (1986).
33. M. A. Ferrara, P. Dardano, L. De Stefano, I. Rea, G. Coppola, I. Rendina, R. Congestri, A. Antonucci, M. De Stefano, and E. De Tommasi, "Optical properties of diatom nanostructured biosilica in arachnoidiscus sp: micro-optics from mother nature," PLoS One **9**(7), e103750 (2014).

Optical Materials EXPRESS

34. E. De Tommasi, I. Rea, V. Mocella, L. Moretti, M. De Stefano, I. Rendina, and L. De Stefano, "Multi-wavelength study of light transmitted through a single marine centric diatom," Opt. Express **38**(6), 1132–1142 (2002).
35. S. G. Johnson, S. Fan, P. R. Villeneuve, J. D. Joannopoulos, and L. A. Kolodziejski, "Guided modes in photonic crystal slabs," Phys. Rev. B **17**(6), 833–839 (1972).
36. L. Cheng, S. Mao, Z. Li, Y. Han, and H. Y. Fu, "Grating couplers on silicon photonics: design principles, emerging trends and practical issues," Micromachines **106**(C7), 14129–14142 (2001).
37. Y. D'Mello, O. Reshef, S. Bernal, E. El-fiky, Y. Wang, M. Jacques, and D. V. Plant, "Integration of sub-wavelength, periodic structures in silicon-on-insulator photonic device design," in *IET Optoelectronics*, (Institution of Engineering and Technology, 2020), pp. 125–135.
38. P. Lalanne and P. Chavel, "Metalenses at visible wavelengths: past, present, perspectives," Laser Photonics Rev. **5**(6), 195–203 (2007).
39. J. Zimmermann, M. Kamp, A. Forchel, and R. März, "Photonic crystal waveguide directional couplers as wavelength selective optical filters," Opt. Commun. **10**(4), 278–288 (2012).
40. J. Upham, B. Gao, L. O'Faolain, Z. Shi, S. A. Schulz, and R. W. Boyd, "Realization of a flat-band superprism on-chip from parallelogram lattice photonic crystals," Opt. Lett. **43**(20), 4981–4984 (2018).
41. E. De Tommasi, E. Esposito, S. Romano, A. Crescitelli, V. Di Meo, V. Mocella, G. Zito, and I. Rendina, "Frontiers of light manipulation in natural, metallic, and dielectric nanostructures," Riv. Nuovo Cim. **44**(1), 1–68 (2021).
42. G. Cohoon, C. Alvarez, K. Meyers, D. Deheyn, M. Hildebrand, K. Kieu, and R. Norwood, *Analysis of Quasi-periodic Pore-Network Structure of Centric Marine Diatom Frustules*, SPIE BiOS (SPIE, 1991), Vol. 28(4), 343–383.
43. M. M. Ghobara, M. A. Tiffany, R. Gordon, and L. Reissig, "Diatom pore arrays' periodicities and symmetries in the euclidean plane: nature between perfection and imperfection," in *Diatom Morphogenesis* (2001), pp. 2929.
44. S. Yoneda, F. Ito, S. Yamanaka, and H. Usami, "Optical properties of nanoporous silica frustules of a diatom determined using a 10 μm microfiber probe," Jpn. J. Appl. Phys. **120**(11), 7381–7399 (2015).
45. K. Vynck, M. Burresi, F. Riboli, and D. S. Wiersma, "Photon management in two-dimensional disordered media," Nat. Mater. **120**(5), 3229–3247 (2015).
46. H. Ding, L. Lalouat, B. Gonzalez-Acevedo, R. Orobtchouk, C. Seassal, and E. Drouard, "Design rules for net absorption enhancement in pseudo-disordered photonic crystal for thin film solar cells," Opt. Express **24**(6), A650–A666 (2016).
47. R. C. Rumpf, J. J. Pazos, J. L. Digaum, and S. M. Kuebler, "Spatially variant periodic structures in electromagnetics," J. Geophys. Res. **75**(15), 2822–2830 (1970).
48. A. Oskooi, P. A. Favuzzi, Y. Tanaka, H. Shigeta, Y. Kawakami, and S. Noda, "Partially disordered photonic-crystal thin films for enhanced and robust photovoltaics," Appl. Phys. Lett. **40**(27), 4885 (2001).
49. J. C. Valmalette, J. Romann, A. Røyset, and M. A. Einarsrud, "3D-hyperspectral mapping of light propagation through diatom frustule silica nanostructures," in *2015 Opto-Electronics and Communications Conference (OECC)*, 2015), 1–3.
50. J. Noyes, M. Sumper, and P. Vukusic, "Light manipulation in a marine diatom," J. Mater. Res. **17**(3), 1535–3235 (2009).
51. C. Maibohm, S. M. M. Friis, M. Ellegaard, and K. Rottwitt, "Interference patterns and extinction ratio of the diatom Coscinodiscus granii," Opt. Express **34**(18), 3477–9548 (1995).
52. K. B. Dossou, "Large field enhancement obtained by combining Fabry–Perot resonance and Rayleigh anomaly in photonic crystal slabs," J. Opt. **35**(9), 1566 (1996).
53. J. W. Goessling, Y. Su, C. Maibohm, M. Ellegaard, and M. Kühl, "Differences in the optical properties of valve and girdle band in a centric diatom," Prog. Oceanogr. **61**(1), 27–56 (2004).
54. L. R. Prelle, M. Albrecht, U. Karsten, P. Damer, T. Giese, J. Jähns, S. Müller, L. Schulz, L. Viertel, and K. Glaser, "Ecophysiological and cell biological traits of benthic diatoms from coastal wetlands of the southern Baltic Sea," Limnol. Oceanogr. **34**(8), 1706–1726 (1989).
55. Y. D'Mello, D. Petrescu, J. Skoric, M. Campbell, M. Andrews, and D. Plant, "Characterization of the Photonic Response in Nitzschia Filiformis Phytoplankton," in *Conference on Lasers and Electro-Optics, OSA Technical Digest* (Optical Society of America, 1908), 377–445.
56. Y. D'Mello, O. Reshef, S. Bernal, E. El-fiky, Y. Wang, M. Jacques, and D. V. Plant, "Integration of periodic, sub-wavelength structures in silicon-on-insulator photonic device design," IET Optoelectron. **65**(11), 2603–2617 (2020).
57. E. D. Palik, *Handbook of Optical Constants of Solids* (Academic Press, 1998), Vol. 3.
58. S. Berthier and J. Lafait, "Effective medium theory: Mathematical determination of the physical solution for the dielectric constant," Opt. Commun. **99**(C7), 14269–306 (1994).
59. S. M. Rytov, "Electromagnetic properties for a finely stratified medium," Limnol. Oceanogr. Lett. **6**(5), 243–252 (2021).
60. M. Florescu, S. Torquato, and P. J. Steinhardt, "Designer disordered materials with large, complete photonic band gaps," Proc. Natl. Acad. Sci. **11**(2), 338–348 (2009).
61. Y. D'Mello, J. Skoric, S. Xu, M. Akhras, P. J. R. Roche, M. A. Lortie, S. Gagnon, and D. V. Plant, "Autocorrelated Differential Algorithm for Real-Time Seismocardiography Analysis," IEEE Sens. J. **19**(13), 5127–5140 (2019).

Optical Materials EXPRESS

62. R. Dhama, V. Caligiuri, L. Petti, A. R. Rashed, M. Rippa, R. Lento, R. Termine, H. Caglayan, and A. De Luca, "Extraordinary effects in quasi-periodic gold nanocavities: enhanced transmission and polarization control of cavity modes," ACS Nano **12**(1), 504–512 (2018).
63. D. Vobornik and S. Vobornik, "Scanning near-field optical microscopy," Bosnian J. Basic Med. Sci. **91**(3), 63–71 (2021).
64. B. Hecht, B. Sick, U. P. Wild, V. Deckert, R. Zenobi, O. J. F. Martin, and D. W. Pohl, "Scanning near-field optical microscopy with aperture probes: fundamentals and applications," Journal of Plankton Research **33**(1), 3–12 (2011).
65. M. Hildebrand, "Diatoms, biomineralization processes, and genomics," Chem. Rev. **108**(11), 4855–4874 (2008).
66. W. Fu, A. Chaiboonchoe, B. Khraiwesh, M. Sultana, A. Jaiswal, K. Jijakli, D. R. Nelson, A. a. Al-Hrout, B. Baig, A. Amin, and K. Salehi-Ashtiani, "Intracellular spectral recompositioning of light enhances algal photosynthetic efficiency," Sci. Adv. **67**(8), 1865–1878 (2022).
67. B. Schellenberger Costa, A. Jungandreas, T. Jakob, W. Weisheit, M. Mittag, and C. Wilhelm, "Blue light is essential for high light acclimation and photoprotection in the diatom Phaeodactylum tricornutum," J. Exp. Bot. **126**(12), 483–493 (2021).
68. J. W. Goessling, P. Cartaxana, and M. Kühl, "Photo-protection in the centric diatom Coscinodiscus granii is not controlled by chloroplast high-light avoidance movement," J. Appl. Phys. **22**(10), 1242–1246 (1951).
69. C. Brunet, R. Chandrasekaran, L. Barra, V. Giovagnetti, F. Corato, and A. V. Ruban, "Spectral radiation dependent photoprotective mechanism in the diatom pseudo-nitzschia multistriata," PLOS ONE **9**(1), e87015 (2014).
70. L. A. Edgar, J. D. Pickett-Heaps, and G. E. Fogg, "The mechanism of diatom locomotion. I. An ultrastructural study of the motility apparatus," Proc. R. Soc. London, Ser. B **88**(1-3), 149–161 (2004).
71. M. Florescu, P. J. Steinhardt, and S. Torquato, "Optical cavities and waveguides in hyperuniform disordered photonic solids," Phys. Rev. B **345**(6272), 242–244 (1990).
72. K. McGarvey-Lechable and P. Bianucci, "Maximizing slow-light enhancement in one-dimensional photonic crystal ring resonators," Opt. Express **22**(21), 26032–26041 (2014).
73. I. Ricárdez-Vargas, M. D. Iturbe-Castillo, R. Ramos-García, K. Volke-Sepúlveda, and V. Ruíz-Cortés, "Hollow spheres as individual movable micromirrors in optical tweezers," Opt. Express **224**, 474–511 (2019).
74. M. Soleimani, L. Rutten, S. P. Maddala, H. Wu, E. D. Eren, B. Mezari, I. Schreur-Piet, H. Friedrich, and R. A. T. M. van Benthem, "Modifying the thickness, pore size, and composition of diatom frustule in Craspedostauros sp. with Al^{3+} ions," Sci. Rep. **100**(9), 1775–1794 (2019).
75. W. Emkey and C. Jack, "Analysis and evaluation of graded-index fiber lenses," J. Lightwave Technol. **6**(3), 323–330 (2016).
76. A. Saha, E. Maria, and M. Z. Baten, "Spectra dependent photonic structure design for energy harvesting by indoor photovoltaic devices," AIP Adv. **57**(7), 1705 (2018).
77. E. De Tommasi and A. C. De Luca, "Diatom biosilica in plasmonics: applications in sensing, diagnostics and therapeutics [Invited]," Biomed. Opt. Express **18**(6), 691–697 (2014).
78. T. Todd, Z. Zhen, W. Tang, H. Chen, G. Wang, Y.-J. Chuang, K. Deaton, Z. Pan, and J. Xie, "Iron oxide nanoparticle encapsulated diatoms for magnetic delivery of small molecules to tumors," Nanoscale **6**(4), 2073–2076 (2014).
79. M. J. Khan, A. Pugazhendhi, B. Schoefs, J. Marchand, A. Rai, and V. Vinayak, "Perovskite-based solar cells fabricated from TiO2 nanoparticles hybridized with biomaterials from mollusc and diatoms," Chemosphere **14**(8), 3602 (2006).
80. A. Rai, M. J. Khan, A. Ahirwar, R. Deka, N. Singh, B. Schoefs, J. Marchand, S. Varjani, and V. Vinayak, "Hydrogen economy and storage by nanoporous microalgae diatom: special emphasis on designing photobioreactors," *Int. J. Hydrogen Energy* (2022).
81. P. Bombelli, A. Savanth, A. Scarampi, S. J. L. Rowden, D. H. Green, A. Erbe, E. Årstøl, I. Jevremovic, M. F. Hohmann-Marriott, S. P. Trasatti, E. Ozer, and C. J. Howe, "Powering a microprocessor by photosynthesis," Energy Environ. Sci. **15**(6), 2529–2536 (2022).
82. L. McMillon-Brown, "Chapter Eleven - Biomimetic advances in photovoltaics with potential aerospace applications," in *Biomimicry for Aerospace*, V. Shyam, M. Eggermont, and A. F. Hepp, eds. (Elsevier, 2022), pp. 291–329.

Supplemental Document

Optical Materials EXPRESS

Solar energy harvesting mechanisms of the frustules of *Nitzschia filiformis* diatoms: supplement

YANNICK D'MELLO,[1,*] SANTIAGO BERNAL,[1] DAN PETRESCU,[2] JAMES SKORIC,[1] MARK ANDREWS,[2] AND DAVID V. PLANT[1]

[1]*Department of Electrical and Computer Engineering, McGill University, Montreal, Quebec, Canada*
[2]*Department of Chemistry, McGill University, 845 Sherbrooke St W, Montreal QC H3A 0G4, Canada*
[*]*Yannick.DMello@mail.McGill.ca*

Supplement DOI: https://doi.org/10.6084/m9.figshare.21466689

Parent Article DOI: https://doi.org/10.1364/OME.473109

Solar energy harvesting mechanisms of the frustules of *Nitzschia filiformis* diatoms: supplemental document

YANNICK D'MELLO[1,*], SANTIAGO BERNAL[1], DAN PETRESCU[2], JAMES SKORIC[1], MARK ANDREWS[2], AND DAVID V. PLANT[1]

[1]*Department of Electrical and Computer Engineering, McGill University, Montreal, Quebec, Canada.*
[2] *Department of Chemistry, McGill University, 845 Sherbrooke St W, Montreal QC H3A 0G4, Canada.*
**Yannick.DMello@mail.McGill.ca*

1. Optical Confinement in Biosilica

The frustule was predominantly made of biosilica. Its refractive index was slightly higher than the surrounding water or inner cytoplasm. Due to this low index contrast and the thinness of the frustule, optical modes were only weakly confined to it. The number of modes and their confinement depended on the thickness, width, and perforation of the frustule as well as the wavelength of the mode. Regions that were perforated with holes had lower effective refractive index [1-3]. The E-field distributions of some of the lower order modes in the frustule are shown in Fig. S1.

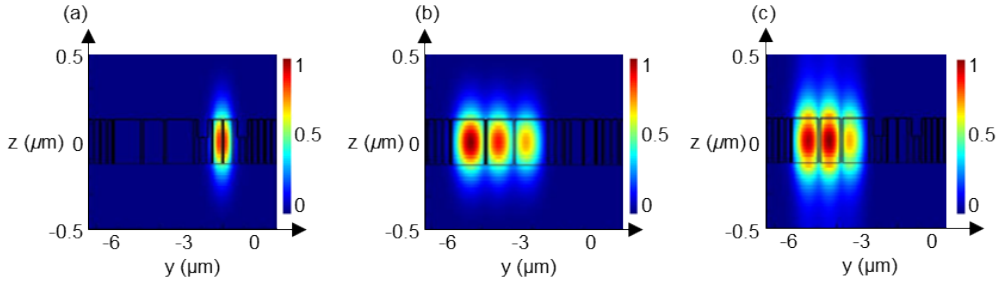

Fig. S1. Mode confinement in the frustule. (a) Fundamental mode inside the valve. (b) Lower order modes inside the girdle. (c) Higher order modes inside the girdle.

Due to weak confinement, the mode field expanded over a larger region such that it penetrated inside the cell. This high overlap facilitated evanescent coupling to the chloroplasts [4, 5] as well as directional coupling to adjacent frustules. Coupling to the chloroplasts was further supported by the marginally higher refractive index of the cytoplasm compared to water, which shifted the field distribution toward the inside of the cell. The location of the chloroplasts inside the cell was found to be variable. Outside the cell, directional coupling with neighboring frustules indicated a mechanism for light to be shared across diatoms in a colony. The weak mode confinement was also found to reduce birefringence resulting in a polarization independent optical response (characterized in Fig. S2(f)), which is beneficial for harvesting unpolarized sunlight.

2. Variations in the Photonic Band Structure of the Central Lattice

The central lattice occupied almost the entire exposed surface area of the valve and therefore, the majority of the frustule. This indicated the higher proportion of incident sunlight that it received in comparison to the other regions of the frustule. The lattice exhibited cylindrical holes from the outside. On the inside, they were covered by 10-nm-thick elliptical protrusions. The knobs were assumed to be artifacts from sputter coating the sample in preparation for scanning electron microscopy (SEM) imaging because otherwise, they would have fatally restricted chemical exchanges between the cell and its environment.

The arrangement of holes in the lattice formed a quasi-periodic photonic crystal (PhC). Different localized regions of the PhC exhibited different symmetries resembling square, triangular, and an intermediate oblique, depending on the angle subtended between the holes. Their corresponding photonic band structures are shown in Fig. S2(a). To quantify the effect of disorder in the PhC, its lattice parameters were varied to produce corresponding variations in the photonic band structure. Using the oblique symmetry as a basis, the dependence of the band structure on variations in angle (or symmetry), refractive index, thickness, spacing, hole diameter, and the polarization of light are shown in Fig. S2. To isolate the effect of a given parameter variation on the overall photonic band structure, only the selected parameter was varied while the others were held constant. The range of the spacing, hole diameter, and thickness parameter variations was two standard deviations from their mean value, that is, 2σ as obtained from the SEM measurements.

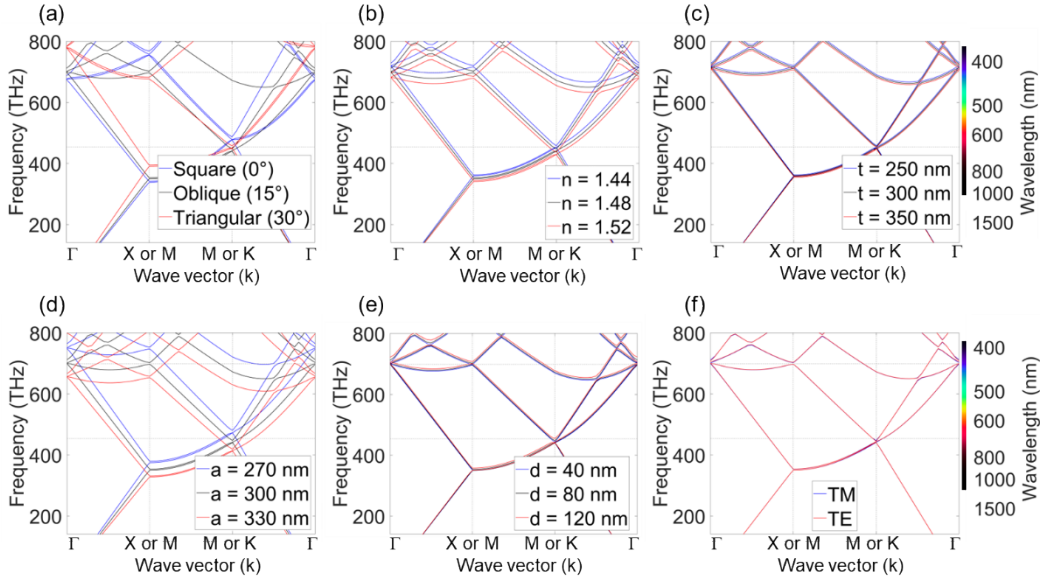

Fig. S2. Dependence of the photonic band diagram on the lattice parameters. Variations in (a) symmetry (corresponding to angle), (b) refractive index, n, (c) thickness, t, (d) spacing, a, (e) diameter, d, and (f) polarization.

For the valve, its guided modes were represented by the bands that were within the light cone of the photonic band structure. Their behavior depended on the localized parameters of the lattice. The strongest variations in the PhC response were due to the lattice symmetry, which could explain the high disorder in the angle between holes despite the longitudinal symmetry of the lattice. This also caused disorder in the spacing between holes. For example, an increase of 20 nm in the spacing proportionally lowered the position of the guided modes by 57 nm toward longer wavelengths. Varying the hole diameter resulted in a similar albeit weaker effect. Diameter variations of up to 100% (or 80 nm) still did not significantly shift the bands. The negligible effect of thickness [6] was attributed to the weak confinement of the modes. Varying the refractive index also had a negligible effect on the response, which justified approximating the biosilica material of the frustule as standard silica. Similarly, the negligible effect of polarization indicated the polarization independence of the optical response. This polarization insensitivity conferred an advantage on the frustule in the context of harvesting sunlight, which is unpolarized.

The central lattice exhibited long-range order despite having no translational symmetry due to the randomized variations of its parameters. This short-range disorder therefore modified the optical response of the PhC without eliminating it [7, 8]. As shown in Fig. S2, any variation of

the periodicity of the lattice induced a proportional change in its corresponding photonic band diagram. So, within a localized region where each unit cell contributed to the overall photonic band structure of the lattice, the disorder of the PhC proportionately shifted the bands into neighboring frequencies, ω, and wavevectors, k (or incident angles), corresponding to their (ω,k) position in the band diagram. This resulted in an effective 'smearing' of the photonic band structure. The effect was visualized in Fig. 2 of the main manuscript, whereby each hole was considered to be a unit cell based on the positions of its neighboring holes, and its corresponding band structure was calculated and plotted. The resulting ensemble average demonstrated an increased likelihood that a mode existed in the PhC to accommodate almost any (ω,k) combination of incident photons.

In this manner, the disorder facilitated random scattering in the lattice. Since the sharpness of peaks in the density of states (DOS) depended on long-range resonant scattering, these peaks got widened and flattened due to the perturbations of the lattice [9]. At each frequency, the DOS was calculated as the sum of all available wavevectors. Since this value depended on the resolution of the simulation, it was normalized within the wavelength range of interest. This broadened the spectrum over which a nonzero (or high) DOS was observed, and therefore increased the range of conditions for which modes were allowed. Additionally, the band gaps were collapsed due to the low refractive index difference, which caused significant overlap between neighboring modes. This effectively smoothed the overall mode field distribution at a given (ω,k) position. As a result, these hybrid modes better overlapped with incident plane waves and therefore, improved free-space coupling to the lattice. The combined DOS similarly increased retention.

The disordered PhC (DPhC) analysis showed that the structure was not only tolerant but in fact benefited from variations, which suggests that they might have evolved to enhance light absorption for a range of wavelengths and incident angles.

3. Resonances of the PhC

The bands in Fig. S2 indicated the modes of the PhC, that is, the allowed optical states for which the DOS was nonzero [10]. Conversely, empty (ω,k) positions in the diagram were indicative of regions in which there were no states for photons to occupy. For example, in the 550-820 nm wavelength range between the X-M symmetry points, the lowest order mode ran parallel to a higher order mode. Their proximity allowed an overlap of their corresponding DOS and field distribution, which averaged these quantities between both modes within that (ω,k) region. Such a combined mode field distribution offered a better overlap with incident light and therefore improved the coupling efficiency of the lattice. The modes also increased the overall DOS available for retention and waveguiding. Similarly, in the shorter wavelength range, the presence of multiple higher order radiation modes increased the coupling efficiency [11, 12]. However, this did not imply better retention in the frustule due to their position outside the light cone.

Positions in the band diagram where the slope of the band approached zero, implied a reduced group velocity [10]. Such regions typically occurred at band gaps or crossings near symmetry points. A band crossing was composed of at least two bands which crossed each other with a low, and possibly zero, slope. In contrast, a gap was composed of at least two bands near each other but not crossing. The width of the gaps in the central lattice were collapsed due to the low refractive index contrast and small hole diameter. For example, at 430 nm in Fig. S3(a), there was a convergence of multiple modes at the Γ point. The reduced slope and group velocity, combined with the presence of multiple bands, indicated a high DOS in those regions. This effect was amplified by the collapsed gap width, as seen at 900 nm. Here, the DOS was not reduced to zero between the bands, as it was for a typical band gap. On the contrary, these collapsed gaps allowed photon tunneling between the modes and therefore resulted in the DOS reaching a peak at the gap rather than on either side of it. An analogy in the spatial domain is a directional coupler, in which the separation between two waveguides can be small enough to

allow evanescent coupling between them, but when the separation is even smaller, then this results in a slot waveguide in which the intensity is actually higher inside the slot [13]. In this manner, the band gaps and crossings supported a continuously high DOS across the spectrum of photosynthetic active radiation (PAR), which contributed to the resonant behavior of the DPhC, as shown in Fig. S3.

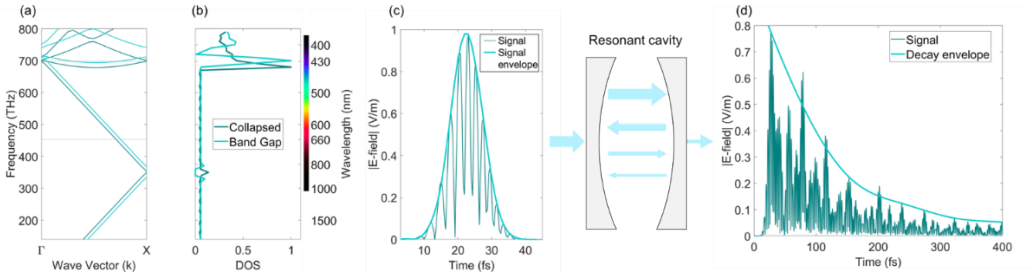

Fig. S3. Effect of resonances on the optical response. (a) Collapsed or open pseudogaps and band crossings with (b) their corresponding DOS. (c,d) Transient response of a resonance (represented by the resonant cavity) showing how (c) an optical pulse undergoes (d) decay due to the retention of light inside the cavity.

The resonances (collapsed pseudogap or band crossing) increased photon lifetimes [14] because photons remained confined or scattered in the frustule for longer durations, as depicted in Fig. S3. Hence, the retention of light by a collapsed pseudogap was more effective than if the gap was widened. Additionally, these resonances enlarged the localized DOS by reducing the group velocity and offering multiple modes for coupling, which increased the coupling efficiency. The increased light retention, light-matter interaction, and coupling efficiency to modes, all directly supported retention in the frustule which could assist the absorption rate of chloroplasts (from evanescent states [15]). In this manner, the resonances in the PhC contributed to the capture, redistribution, and retention of incident PAR.

4. Analysis of Scanning, Near-field Optical Microscopy (SNOM) Images

SNOM is a surface selective technique, which can be used to probe diatom frustules due to their transparency and thinness. Evanescent waves were coupled from the aperture to the sample in the near field at a fixed angle, which implied that the interaction for each pixel occurred only at the tip. During scanning, a constant separation between the tip and sample was maintained to ensure constant coupling despite the exponential decay of the wave with increasing separation distance [16]. Although SNOM is non-destructive, the tip itself damaged the sample in some cases.

In this transmission SNOM configuration, incident light was evanescently coupled into the sample by the apertured probe above it [16]. The amount of light coupled into the sample depended on the focal length of the lens and size of the aperture in the cantilever, both of which had a spectrally dependent optical response. This implied that long wavelengths (near infrared) were limited by the aperture size whereas short wavelengths (near violet) did not reach the aperture due to the correspondingly shorter focal length of the lens. Once coupled to the sample, the transmitted light was detected via an objective lens beneath it. The regions around the valve where light had coupled to, but diffused through, the cover slip provided a baseline intensity. Compared to this background, darker regions in the frustule indicated that light had not been transmitted to the collection optics. In this case, light had either not coupled into the sample due to poor contact (as seen inside the holes) or was redirected away from the point of contact (as seen in the diffraction pattern outside the valve edges). In contrast, the bright points indicated higher transmission through the sample, that is, where light was efficiently coupled to the valve without being diffused or redirected. A collection of these points formed bright lines which

were observed along the valve edges as well as laterally across the width of the central lattice. These continuous pathways indicated waveguiding.

The accuracy of the probed optical response was constrained by the measurement technique. For example, the angle at which the aperture was tapered, determined the fidelity of images obtained from surfaces with high curvature. Near the edges of the valve, the field was noticeably darker because the outer edge of the cantilever was physically restricted by its contact with the edge of the valve. As a result, the separation between the tip and the surface could not be maintained, which was confirmed by the blurriness of the AFM image. Similar dark spots were observed between the scaffolds of the raphe. Additionally, the convergence semi-angle of the bottom objective determined the aggregate of all k-vectors which were collected around the Γ symmetry point of the lattice. Hence, SNOM only probed the k-vectors around the Γ symmetry point for a single wavelength. However, note that the tip excited all modes in the lattice even if only the Γ symmetry point was preferred. Hence, light also coupled to modes that existed at other k-vectors. Due to scattering from imperfections in the lattice, residual light from these existing interacting modes would still reach the bottom objective. As a result, the sample was not dark despite the lack of modes at the Γ point for the SNOM wavelength, but the modes can be expected to appear brighter if probed at the correct angle. To do so, the angle of the detector would need to be adjustable, along with a sweep of the wavelengths within the range of PAR. The lack of mobility in our setup prevented the mapping optical bands in this manner.

Note that SNOM images did not produce a direct measurement of the localized DOS (LDOS) due to cross-coupling between the tip and sample [17]. However, given the experimental conditions and expected topography of the sample, the LDOS was inferred to have some correlation with bright pixels in the image. That is, the partial LDOS can be reconstructed from variations in the transmitted intensity resulting from the interactions between the aperture and the sample [18]. This is the sum of the partial DOS associated with the optical modes in each polarization direction, whereby its electric or magnetic part can be correlated with the near-field measurement [19]. So, the bright spots can be interpreted as the probability of detecting the electric field intensity of photons at that position. The bright points therefore indicated a higher LDOS at the point of contact in comparison to the surrounding regions. Since the LDOS indicated the availability of optical eigenmodes that allowed the existence of photons at a specific location, the bright points in the SNOM image were therefore assumed to map out the optical modes in the frustule. However, the total LDOS was not directly measured due to the vectoral nature of the optical field [19], which required a much larger convergence angles to obtain all k-vectors. Hence generalization was not straightforward. A complete LDOS measurement is only possible if all the modes are excited as well as detected, that is, illumination and detection by a wide solid angle. This was not possible using SNOM, hence, the image was generally interpreted as representing the k-vectors for the given laser wavelength, and possibly around the Γ symmetry point.

5. Photonic Circuit Model of the Frustule

The photosynthetic conversion efficiency of the diatom cell was assumed to match the absorption rate of its chloroplasts. The chloroplasts could receive incident PAR from the frustule via either direct transmission or evanescent coupling. Our results indicate that the frustule contributed to the PAR harvesting mechanisms of capture, redistribution, and retention. Each of these mechanisms was caused by a combination of the localized optical functionalities that were evoked by its architecture. We modeled this process as a photonic circuit, which is represented in Fig. S4(a). An analogous, simplified electrical circuit of this system is shown in Fig. S4(b) and its effect on photosynthesis is depicted in Fig. S4(c).

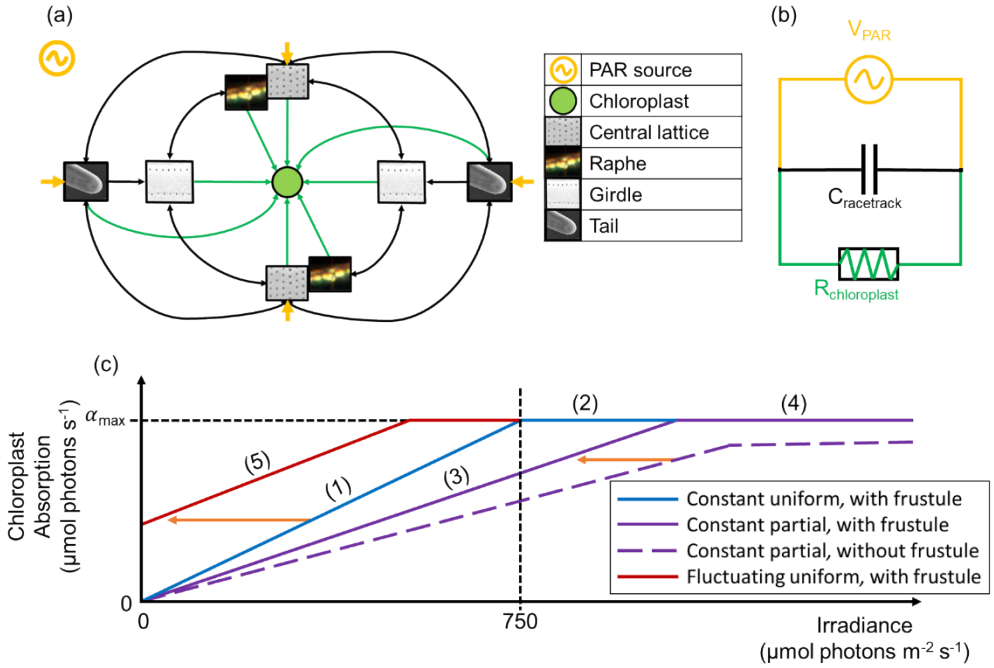

Fig. S4. Model of the optical response of the frustule. (a) Photonic circuit of the frustule showing (yellow arrows) incident PAR, (black arrows) light exchanged between different regions and (green arrows) absorption by the chloroplasts. (b) Electrical equivalent circuit with the chloroplasts, frustule, and PAR represented as a load resistor, capacitor, and variable power supply, respectively. (c) Contribution of the frustule to the absorption by the chloroplasts depending on the amount and distribution of irradiation on the cell. The slope represents the difference in the exposed surface area. The contribution of the frustule is depicted as orange vertical arrows in specific cases. The maximum absorption α_{max} was reached under an irradiance of 750 μmol photons m^{-2} s^{-1}.

The black, inner ring of Fig. S4(a) represents the cross-sectional racetrack formed by the central lattice, raphe, and girdle, which is shown in Fig. 7(a) of the main manuscript. It retained photons via circulation with an estimated Q factor of 271 to 822 at the wavelengths of 805 nm to 424.8 nm. For simplicity, this was assumed to be the main cause of retention in the frustule since the contributions from the raphe and DPhC merely amplified this effect. The remaining black arrows in Fig. S4(a) show how the racetrack received light via either butt-coupling from the tails or diffraction from the DPhCs in the central lattice and girdle. The radiation modes of the DPhC allowed light to couple into the racetrack from free-space with a simulated insertion loss (IL) of 4.56 dB at 450 nm [20]. Butt-coupling at the tail resulted in a simulated IL of 1.4 dB with free-space. Note that this is the approximate maximum value since the light source was aligned with the tail to obtain the lowest IL. For light being diffracted into lateral circulation by the central lattice and girdle, it incurred an approximately 7 dB loss [20]. Since these features also maintained lateral circulation by limiting longitudinal diffusion toward the tails, the loss from diffusion was neglected. The effective index of the racetrack was approximated as 1.38. Its optical loss per roundtrip was therefore calculated as,

$$Loss_{\text{racetrack}} = \frac{2\pi f T_{\text{r}}}{Q} \tag{S1}$$

Here, f is the frequency, T_{r} is the transient time of the ring, and Q is its quality factor. This loss was calculated to be 2.6 dB per roundtrip.

The contribution of the capture, redistribution, and retention mechanisms depended on the initial state and boundary conditions of the system, which are represented in Fig. S4(c). We therefore present the following qualitative analysis of the contribution of the frustule to the absorption of chloroplasts using 5 cases which are based on the amount, location, and consistency of PAR that is incident on the diatom. Note that in all cases, the capture mechanism can be assumed to be always active and is therefore not discussed.

1. Under a constant, low, uniform irradiance (blue, solid, sloping line in Fig. S4(c)), any light in the frustule is immediately absorbed by the chloroplasts, which renders the retention mechanism redundant. Since the irradiance is uniform, the redistribution mechanism is also redundant. Hence, only the capture mechanism is useful to couple ambient light.
2. Under a constant, high, uniform irradiance (blue, solid, horizontal line in Fig. S4(c)), absorption of the chloroplasts is maximized, so excess photons are retained in the frustule. Although retention is activated, it is not used because these photons cannot be absorbed by the chloroplasts while they are already saturated. Similar to case 1, the uniformity of the irradiance renders the redistribution mechanism as redundant.
3. Under a constant, low, partial irradiance (purple, sloping lines in Fig. S4(c)), any captured light gets absorbed. A fraction might be redistributed for absorption by chloroplasts in the remaining regions of the cell, but this is only due to the passive optical behavior of the frustule rather than the presence of excess photons. Similar to case 1, the low irradiance renders the retention mechanism as redundant.
4. Under a constant, high, partial irradiance (purple, horizontal lines in Fig. S4(c)), the illuminated area of the cell absorbs photons at its maximum capacity until the chloroplasts are saturated. Excess photons can be made available to the remaining chloroplasts via the capture and redistribution mechanisms. This increases photosynthetic conversion in the cell. Similar to case 2, the retention mechanism is activated but not used.
5. Under a fluctuation from high to low, uniform irradiance (red, solid line in Fig. S4(c)), as represented by $t > 0$, the retention mechanism is most useful. Excess photons retained in the frustule are available to the chloroplasts so that photosynthesis can continue despite a drop in irradiance.

The redistribution mechanism was found to be useful when the frustule is partially irradiated. Since it effectively increases the exposed surface area under irradiation, it was represented by an increase in the slope of the corresponding lines in Fig. S4(c). Redistribution across the frustule allowed us to make an analogous assumption that the chloroplasts were distributed throughout the cell. The retention mechanism gets activated when the irradiation exceeds the maximum absorption of the chloroplasts and becomes useful when the irradiation drops below the maximum. Since it provides a smoothing effect during fluctuations in irradiance by releasing stored optical energy during periods of darkness, it was represented by a positive offset of the corresponding lines in Fig. S4(c). The adaptations of chloroplasts to available light were not accounted for in this model.

This retention mechanism was additionally modeled by a capacitor (the frustule) connected in parallel with a resistive load (the chloroplasts) to smoothen spikes or cuts in the power supply (incident irradiance). Similar to a resistor, the maximum absorption rate of chloroplasts, $\alpha_{\max}$, was assumed to be a constant 3.98×10^{12} photons/s using an irradiance of 750 μmol photons m^{-2} s^{-1} at 440 nm [21]. It was calculated as,

$$\alpha_{\max} = IA\epsilon \tag{S2}$$

Here, I is the maximum irradiance, A is the surface area of the frustule, and ϵ is the absorbance coefficient of the chloroplasts approximated as 1 dB [20]. To find the contribution of the frustule to photosynthesis, we calculated the contribution of the racetrack to α. We assumed that all the

photons retained in the frustule were available for absorption by the chloroplasts at any time, that is, the retention rate, $Rate_{\text{retained}} = 1 - Rate_{\text{leak}}$, determined the maximum photons per second available for absorption. The leakage or decay rate, $Rate_{\text{leak}}$ was calculated using the total rate of photons/s that coupled into the racetrack due to the initial irradiance and harvesting mechanisms as well as $Loss_{\text{racetrack}}$.

For an irradiance of 550 µmol photons m^{-2} s^{-1}, the $Rate_{\text{retained}}$ that enabled $\alpha \rightarrow \alpha_{\max}$ was calculated as 0.319×10^{12} photons/s. The total contribution to photosynthesis provided by the frustule was then estimated as $Rate_{\text{retained}}/\alpha_{\max}$ because this represented the percentage increase in α due to the retention mechanisms of the frustule. It was found to be 9.83% at a wavelength of 450 nm. Note that this value represents an estimated percentage increase based on the specified conditions and was only calculated for a single wavelength. The accuracy of the calculation can be improved by conducting a full spectral analysis of the frustule within the wavelength range of PAR.

References

1. J. W. Goessling, W. P. Wardley, and M. Lopez-Garcia, "Highly Reproducible, Bio-Based Slab Photonic Crystals Grown by Diatoms," Advanced Science **7**, 1903726 (2020).
2. S. Berthier and J. Lafait, "Effective medium theory: Mathematical determination of the physical solution for the dielectric constant," Optics Communications **33**, 303-306 (1980).
3. S. M. Rytov, "Electromagnetic Properties fo a Finely Stratified Medium," JETP **2**, 466-475 (1956).
4. E. De Tommasi, "Light Manipulation by Single Cells: The Case of Diatoms," Journal of Spectroscopy **2016**, 13 (2016).
5. J. W. Goessling, Y. Su, P. Cartaxana, C. Maibohm, L. F. Rickelt, E. C. L. Trampe, S. L. Walby, D. Wangpraseurt, X. Wu, M. Ellegaard, and M. Kühl, "Structure-based optics of centric diatom frustules: modulation of the in vivo light field for efficient diatom photosynthesis," New Phytologist **219**, 122-134 (2018).
6. K. Vynck, M. Burresi, F. Riboli, and D. S. Wiersma, "Photon management in two-dimensional disordered media," Nature Materials **11**, 1017 (2012).
7. Z. V. Vardeny, A. Nahata, and A. Agrawal, "Optics of photonic quasicrystals," Nature Photonics **7**, 177-187 (2013).
8. D. S. Wiersma, "Disordered photonics," Nature Photonics **7**, 188 (2013).
9. Z.-Y. Li and Z.-Q. Zhang, "Fragility of photonic band gaps in inverse-opal photonic crystals," Physical Review B **62**, 1516-1519 (2000).
10. Y. D'Mello, O. Reshef, S. Bernal, E. El-fiky, Y. Wang, M. Jacques, and D. V. Plant, "Integration of Sub-wavelength, Periodic Structures in Silicon-on-Insulator Photonic Device Design," in *IET Optoelectronics,* (Institution of Engineering and Technology, 2020), pp. 125-135.
11. T. Fuhrmann, S. Landwehr, M. El Rharbi-Kucki, and M. Sumper, "Diatoms as living photonic crystals," Applied Physics B **78**, 257-260 (2004).
12. Y. Tang, Z. Wang, L. Wosinski, U. Westergren, and S. He, "Highly efficient nonuniform grating coupler for silicon-on-insulator nanophotonic circuits," Optics Letters **35**, 1290-1292 (2010).
13. V. R. Almeida, Q. Xu, C. A. Barrios, and M. Lipson, "Guiding and confining light in void nanostructure," Optics Letters **29**, 1209-1211 (2004).
14. Y. D'Mello, S. Bernal, J. Skoric, D. Petrescu, M. Andrews, and D. V. Plant, "Photonic Crystal Behavior of Nitzschia Filiformis Phytoplankton for Chlorophyll A Photosynthesis," in *Conference on Lasers and Electro-Optics*, OSA Technical Digest (Optical Society of America, 2019), JW2A.121.
15. J. D. Joannopoulos, S. G. Johnson, J. N. Winn, and R. D. Meade, *Photonic Crystals: Molding the Flow of Light,* 2 ed. (Princeton University Press, 2008).
16. B. Hecht, B. Sick, U. P. Wild, V. Deckert, R. Zenobi, O. J. F. Martin, and D. W. Pohl, "Scanning near-field optical microscopy with aperture probes: Fundamentals and applications," The Journal of Chemical Physics **112**, 7761-7774 (2000).
17. C. Huang, A. Bouhelier, G. C. des Francs, G. Legay, J. C. Weeber, and A. Dereux, "Far-field imaging of the electromagnetic local density of optical states," Optics Letters **33**, 300-302 (2008).
18. C. Chicanne, T. David, R. Quidant, J. C. Weeber, Y. Lacroute, E. Bourillot, A. Dereux, G. Colas des Francs, and C. Girard, "Imaging the Local Density of States of Optical Corrals," Physical Review Letters **88**, 097402 (2002).
19. C. Girard, T. David, C. Chicanne, A. Mary, G. C. d. Francs, E. Bourillot, J. C. Weeber, and A. Dereux, "Imaging surface photonic states with a circularly polarized tip," Europhysics Letters (EPL) **68**, 797-803 (2004).
20. S. Yoneda, F. Ito, S. Yamanaka, and H. Usami, "Optical properties of nanoporous silica frustules of a diatom determined using a 10 µm microfiber probe," Japanese Journal of Applied Physics **55**, 072001 (2016).

21. J. W. Goessling, S. Frankenbach, L. Ribeiro, J. Serôdio, and M. Kühl, "Modulation of the light field related to valve optical properties of raphid diatoms: implications for niche differentiation in the microphytobenthos," Marine Ecology Progress Series **588**, 29-42 (2018).